JOURNAL OF GEOPHYSICAL RESEARCH, VOL. 102, NO. B4, PAGES 7783–7802, APRIL 10, 1997

Three-dimensional structure of asthenospheric flow beneath the Southeast Indian Ridge

Brian P. West, William S. D. Wilcock, and Jean-Christophe Sempéré[1]

School of Oceanography, University of Washington, Seattle

Louis Géli

Département de Géosciences Marines, Institut Français de Recherche pour l'Exploitation de la Mer, Plouzané, France

Abstract. Both geophysical and geochemical evidence suggests the presence of along-axis asthenospheric flow toward the Australian-Antarctic Discordance (AAD) beneath the Southeast Indian Ridge (SEIR). We use a three-dimensional, finite-volume formulation of viscous flow to investigate the structure of asthenospheric motion beneath the SEIR. Our results show that simple continental separation in either a constant- or variable-viscosity mantle without horizontal temperature gradients is unable to reproduce the inferred asthenospheric flow velocities and observed geographic distribution of the "Indian" and "Pacific" upper mantle isotopic provinces. The presence of a cooler, more viscous mantle directly beneath the AAD is necessary to reproduce observed constraints. High viscosities beneath the AAD induce significant along-axis flow beneath the neighboring SEIR that advects warmer material over the cooler, more viscous mantle. In passive flow models, a temperature anomaly of about 300°C at a 400-km depth is required. Simulations that include the effects of buoyancy forces reduce the required temperature anomaly to 100°-200°C, a result in good agreement with other estimates of the regional temperature anomaly. These models also match observed near-axis variations in residual depth and crustal thickness. In both passive and buoyant simulations, the presence of high-viscosity (cooler) upper mantle beneath the AAD results in reduced upwelling, consistent with low extents of decompressional melting inferred from geochemical and geophysical constraints. Along-axis flow acts to subdue temperature variations within the melting region relative to the deeper mantle and results in a temperature inversion in the subaxial asthenosphere. This effect may also reduce the variations in geochemical parameters such as $Na_{8.0}$ and $Fe_{8.0}$ with axial depth below those observed in global correlations.

Introduction

The present-day Southern Ocean formed via the rifting of Gondwana, beginning around 100 Ma at the western end of Australia and then propagating eastward at approximately 2 cm yr^{-1} [*Mutter et al.*, 1985; *Cande and Mutter*, 1982]. Unlike other boundaries of Gondwana, the rifting of Australia and Antarctica was not a direct result of hot-spot influence and is associated with the long-term presence of cooler than normal upper mantle temperatures [*Veevers*, 1982]. Initial spreading between the two continents occurred at an extremely slow half rate of 2-6 mm yr^{-1} from 96 Ma until 45-43 Ma and then accelerated to an average half rate of 30-35 mm yr^{-1} as significant global plate reorganization occurred [*Mutter et al.*, 1985]. At present, the intermediate spreading Southeast Indian Ridge (SEIR) extends from the Macquarie to the Rodrigues triple junctions, separating the Indo-Australian from the Antarctic plate (Figure 1, inset).

Over the length of the SEIR, significant gradients in mantle temperature are inferred from geochemical and geophysical evidence [*Sempéré et al.*, 1996, 1997]. The Australian-Antarctic Discordance (AAD) lies near the center of the SEIR between the Amsterdam-Kerguelen and Balleny-Tasmantid hotspots (Figure 1, inset). The AAD is a region of unusually thin oceanic crust, rough topography, deep regional bathymetry, and axial depths (Figure 1) and is believed to represent the surface expression of regionally cooler mantle temperatures. To the west of the AAD, the SEIR displays a transition from predominantly axial ridges between 88° and 102° E to a more subdued axial topographic variation between 107° and 114°E [*Sempéré et al.*, 1997]. The axis of the SEIR to the east of the AAD is associated with a 10-km-wide, 500-m-high axial ridge similar to that of the East Pacific Rise (EPR) [*West et al.*, 1994; *Sempéré et al.*, 1996]. In contrast, the SEIR within the AAD is characterized by a 500- to 1500-m-deep, 5- to 20-km-wide rift valley, a feature usually associated with slow-spreading centers [*Palmer et al.*, 1993; *West et al.*, 1994; *Sempéré et al.*, 1996]. Axial depths also vary significantly between 90° and 145°E, ranging from 2500 m near 140°E and 100°E to nearly 4750 m within the AAD (Figure 1). Using a current model of the formation of axial topography [*Chen*, 1996a, b; *Phipps Morgan and Chen*, 1993], these contrasts in axial depth and morphology require thicker crust and warmer mantle temperatures both to the east and west of the AAD.

The geochemical contrasts between the AAD and regions to the east and west along the SEIR are also consistent with the

[1]Now at Exxon Production Research Company, Houston, Texas.

Paper number 96JB03895.
0148-0227/97/96JB-03895$09.00

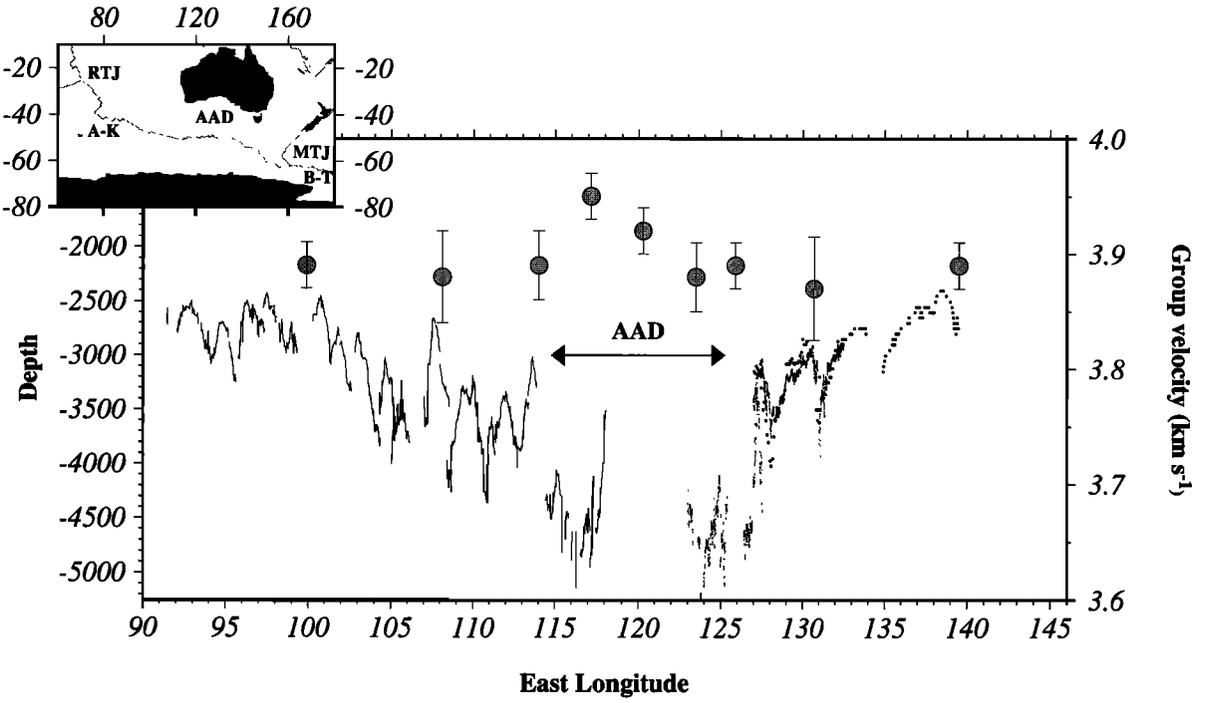

Figure 1. Along-axis depth profile of the Southeast Indian Ridge (SEIR) between 90°E and 145°E (data sources west to east; Sempéré et al. [1997], West et al. [1994], and J. Phipps Morgan, unpublished data, 1995) and averaged Rayleigh wave group velocities (shaded dots, with error bars representing 1 standard deviation) after *Kuo et al.* [1996]. Inset shows geographic locations of the Rodrigues (RTJ) and Macquarie (MTJ) Triple Junctions, Amsterdam-Kerguelen (A-K) and Balleney-Tasmantid (B-T) hotspots, and the Australian-Antarctic Discordance (AAD). Both the depth and surface wave anomalies associated with the AAD suggest that it is a region of relative cool upper mantle temperatures centered near 120°E.

AAD being a region of low melt production and thin crust. The axial valleys of the AAD are characterized by lavas with high $Na_{8.0}$ and low $Fe_{8.0}$, while the axial ridges of the SEIR to the east are characterized by less sodic, more iron-rich lavas [*Pyle*, 1994]. Gradients in geochemical parameters to the west of the AAD also demonstrate that the AAD is a region of low melt production [*Christie et al.*, 1995], although between 98° and 116°E, parameters such as $Na_{8.0}$ and $Fe_{8.0}$ vary more slowly with axial depth than the trends defined by the "global correlation" of *Klein and Langmuir* [1987] [*Christie et al.*, 1995].

Various methods have been used to estimate the temperature anomaly beneath the AAD. *Forsyth et al.* [1987] report that beneath the AAD Rayleigh wave phase velocities in the 20- to 100-s range are significantly faster than for regions of comparable age in the Pacific. The difference of about 0.35 km s^{-1} can be modeled by a mantle temperature difference of less than 100°C and a change in melt fraction of about 8% [*Forsyth*, 1992]. *Kuo* [1993] jointly inverts geoid and topography anomalies of the SEIR and suggests a temperature anomaly of 80° and 250°C beneath the AAD for layers extending to depths of 300 and 100 km, respectively. *West et al.* [1994] estimate a 50° to 100°C variation between segments in the western portion of the AAD and regions of the SEIR immediately to the east, using topographically corrected satellite gravity data and numerical models of mantle flow and melt generation. Isostatic arguments generally fall within the range of 85° to 150°C [*Hayes*, 1988; *Sempéré et al.*, 1997]. Using geochemical methods, *Shen and Forsyth* [1995] deduce a temperature anomaly of not more than about 60°C to explain their trace element systematics. Their model predicts a relatively small variation in the onset of melting and large variation in the final pressure of melting. The *Shen and Forsyth* [1995] estimate is less than the 100° to 150°C variation required by *Klein and Langmuir* [1987], who assume that the final pressure of melting is constant beneath the SEIR between ~100° and 132°E. Thus, while individual estimates may vary significantly, the data are generally compatible with an upper mantle temperature decrease of ~100°C beneath the AAD.

In addition to being associated with relatively cooler mantle temperatures, the AAD has also been postulated as a sink for along-axis asthenospheric flow beneath the SEIR [*Parmentier and Olivier*, 1979; *Vogt et al.*, 1984; *Baumgardner*, 1988; *Alvarez*, 1990; *Marks et al.*, 1990, 1991; *Klein et al.*, 1988; *Kuo*, 1993; *Kuo et al.*, 1995; *Sempéré et al.*, 1996; 1997; B. P. West et al., manuscript in preparation, 1997]. As such, the AAD appears to be a unique portion of the global mid-ocean ridge network since it is associated with both a cooler upper mantle and along-axis flow. *Parmentier and Oliver* [1979] modeled shallow, global mantle circulation due to the accretion and subduction of lithospheric plates and predicted mantle flow around the root of the northward- moving Australian continent. This model is consistent with sublithospheric mantle flow beneath the SEIR that converges on the AAD in the wake of the Australian continent. *Alvarez* [1982, 1990] also proposed that upper mantle flow converges on the AAD around the root of the Australian continent owing to long-term shrinkage of the Pacific Ocean basin. More recently, *Marks et al.* [1990, 1991] suggested that the upper mantle beneath the axis of the SEIR is currently downwelling beneath the AAD, based upon the

pattern of residual depth anomalies and residual geoid to topography ratios.

Conceptual models of mantle flow in and near the AAD fall into essentially two end-member classes: those involving convective flow with possible downwelling beneath the AAD and those involving a passive viscous response to cooler than normal mantle temperatures. The first class assumes either that mantle downwelling is providing dynamic support for the AAD depth anomaly or that material from the Amsterdam-Kerguelen and Balleny-Tasmantid hotspots (Figure 1) is forcing asthenosphere into the AAD [*Marks et al.*, 1990, 1991]. The second class assumes that the depth anomaly is due to local compensation of regionally thin crust with passive along-axis mantle flow to maintain mass continuity over a stiff, cold mantle layer beneath the AAD [*Forsyth et al.*, 1987]. In this study, we examine numerically upper mantle flow that is driven by both continental separation and upper mantle temperature gradients. Our goal is to construct a simple model which can account for the anomalous geochemical and geophysical features of the Southern Ocean and AAD in a physically consistent framework.

Observed Constraints on Upper Mantle Flow Along the SEIR

Geochemical Constraints

The unusual geophysical features of the AAD and surrounding SEIR are associated with a sharp discontinuity in the Sr, Nd, and Pb isotopic signatures of SEIR lavas. This marks the boundary between "Indian" and "Pacific" mid-ocean ridge basalt (MORB) source upper mantle provinces [*Klein et al.*, 1988; *Pyle et al.*, 1992, 1995]. This transition in isotopic signature is presently located near a transform offset of the SEIR between 126.5° and 127°E and extends over less than about 70 km along axis [*Pyle et al.*, 1992]. Off-axis samples dredged from 3-4 Ma seafloor in the easternmost AAD spreading segment record the presence of Indian MORB mantle beneath a segment that is now erupting lavas with Pacific type isotopic characteristics [*Pyle et al.*, 1992]. This change in mantle source signature implies that Pacific mantle has migrated westward beneath the easternmost AAD spreading segment at a minimum rate of 25 mm yr^{-1} for the last 3-4 Myr [*Pyle et al.*, 1992, 1995].

Recent isotopic studies of basalts from Deep Sea Drilling Project (DSDP) sites surrounding the AAD (Legs 28 and 29) (Figure 2) further constrain the relative positions of Pacific and Indian upper mantle at 70 Ma [*Pyle et al.*, 1995], and have been interpreted to support arguments for the long-term westward migration of the isotopic boundary [*Pyle et al.*, 1995]. Samples from several DSDP sites in the SW Pacific, south of New Zealand (Figure 2), appear to be derived from a Pacific mantle source that presumably was present along the eastern margin of Gondwana prior to the rifting of Australia and Antarctica. Furthermore, southeast Indian Ocean DSDP sites between the Kerguelen Plateau and the AAD all have Indian MORB isotopic characteristics. Samples that erupted at two sites along the western margin of the South Tasman Rise are of particular interest; basalts recovered from DSDP hole 280A (~47 Ma seafloor) fall within the field of Indian MORB compositions, while basalts from DSDP hole 282 (~55 Ma seafloor) exhibit moderately Pacific MORB isotopic signatures with compositions that closely resemble transitional samples recovered close to the present-day boundary within the AAD [*Pyle et al.*, 1995]. These data seem to indicate that Indian mantle was present near the western margin of the South Tasman Rise at ~60 Ma (Figure 2), well to the east of the intersection of the residual depth anomaly with the Australian continental margin. In addition, two highly altered 30-40 Ma basalts dredged to the east and north of the AAD (37°46'S, 132°19'E; and 39°55'S, 131°58'E) also have Indian type isotopic ratios (Figure 2) [*Lanyon et al.*, 1995].

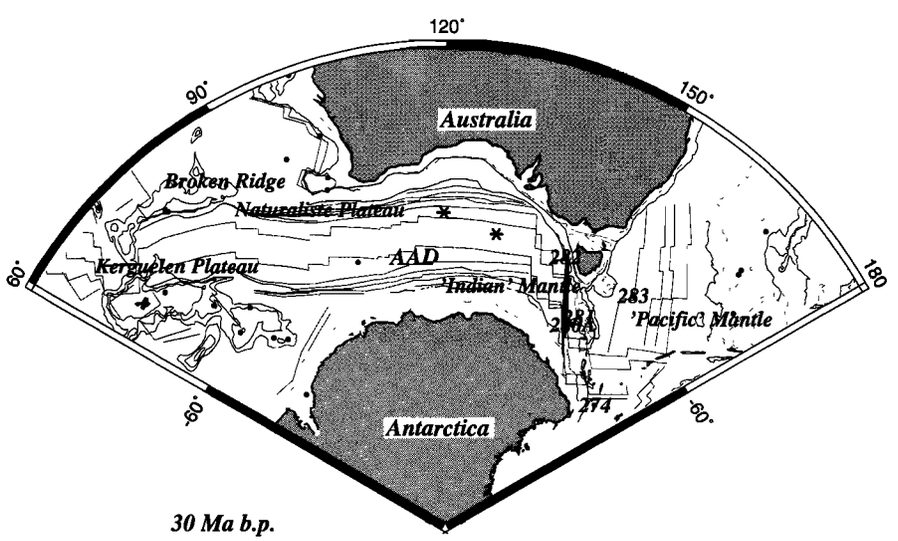

Figure 2. Tectonic reconstruction of the Australian and Antarctic continents to 30 Ma [after *Pyle et al.*, 1995 and *Lawver et al.*, 1992] showing the distribution of Deep Sea Drilling Project (DSDP) sites in this region (dots) and distribution of the Indian and Pacific upper mantle isotopic provinces (noted by text). *Pyle et al.* [1995] suggest that all basalts from DSDP sites east of Tasmania at 30 Ma are derived from a Pacific type upper mantle. Samples from sites 282 and 280A, however, show transitional and Indian mantle sources, respectively, as is currently observed on axis within the AAD. The paleoposition of the *Lanyon et al.* [1995], Indian type samples (stars) are consistent with the *Pyle et al.* [1995] hypothesis.

Although the off-axis data described above are not conclusive [*Pyle et al.*, 1995], they are consistent with the suggestion that Indian type mantle was present far to the east of the AAD at the time when South Tasman Rise separated from Australia, and that this mantle has migrated along axis to its current location within the AAD. Assuming a constant velocity, *Pyle et al.* [1995] suggest that the isotopic boundary has migrated at to its current location at a mean velocity of about 40 mm yr^{-1} since 60 Ma [*Pyle et al.*, 1995] (Figure 3). In addition, the *Lanyon et al.* [1995] samples, which lie to the north-northeast of the AAD, constrain the mean velocity to a minimum of ~20 mm yr^{-1} since 30 Ma. However, other than the *Lanyon et al.* [1995] samples, no geochemical constraints exist on the isotopic boundary from 50 to 5 Ma, and models with variable migration velocities can satisfy the available data.

Geophysical Constraints

Marks et al. [1990, 1991] calculated residual depth anomalies for this region of the Southern Ocean and showed that anomalous seafloor can be traced in a "V"-shaped pattern into both the Australian and Antarctic continents (Figure 4). In addition to suggesting the presence of cooler upper mantle temperatures and/or thinner crust, the V shape of the residual depth anomaly indicates westward motion within the mantle [*Marks et al.*, 1990, 1991]. *Marks et al.* [1991] suggest the off-axis symmetry reflects westward migration of the source of the residual depth anomaly with respect to the axis of the SEIR during the opening of the Southern Ocean (Figure 4). This, in turn, has been interpreted to reflect along-axis asthenospheric flow at a rate of between 15 and 25 mm yr^{-1} that advects the depth anomaly source toward the AAD from the east [*Marks et al.*, 1990].

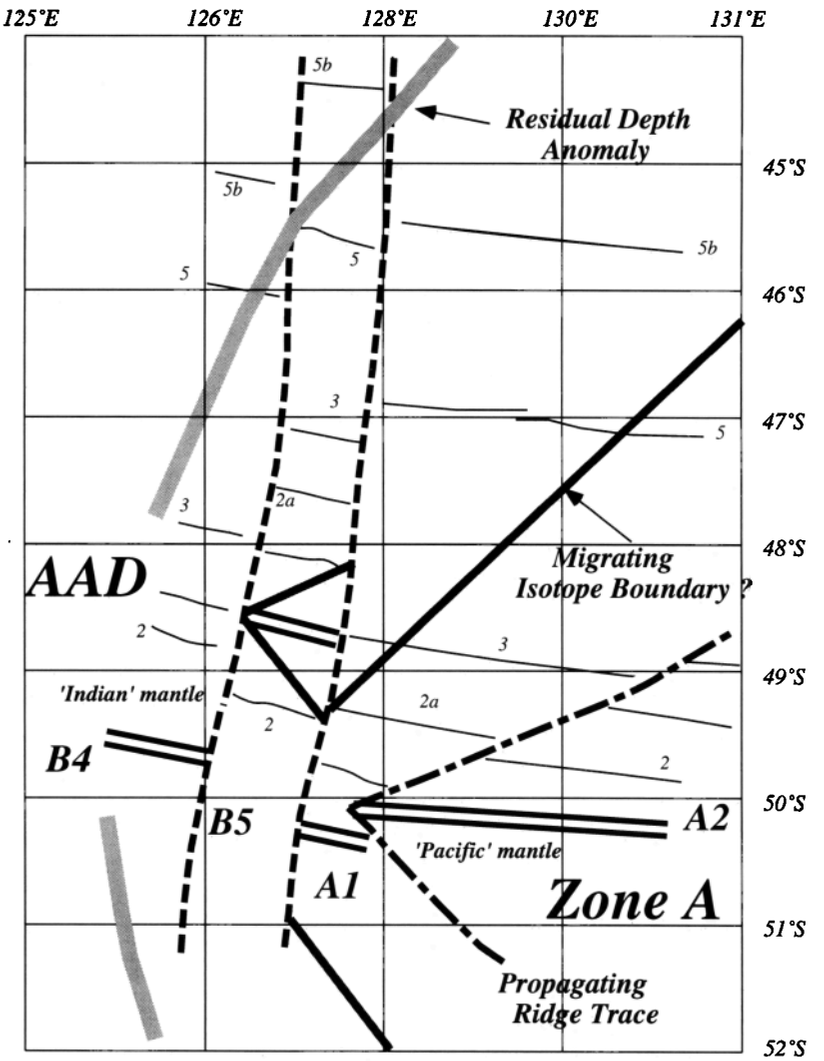

Figure 3. Schematic of constraints on along-axis flow of asthenosphere beneath the SEIR and AAD (modified after *Pyle et al.* [1995]). The isotopic transition between Indian and Pacific upper mantle currently exists at approximately 127°E within the AAD, and the inferred migration of the boundary is recorded by the thick solid line *Pyle et al.* [1995]. The off-axis trace of the residual depth anomaly is taken from *Marks et al.* [1990], and its intersection with the eastern transform of the AAD (dashed line) approximately at magnetic anomaly 5b is coincident with the development of the strongly segmented character of the SEIR within the AAD. Propagating ridge traces also intersect the eastern transform and suggest along-axis motion within the upper mantle.

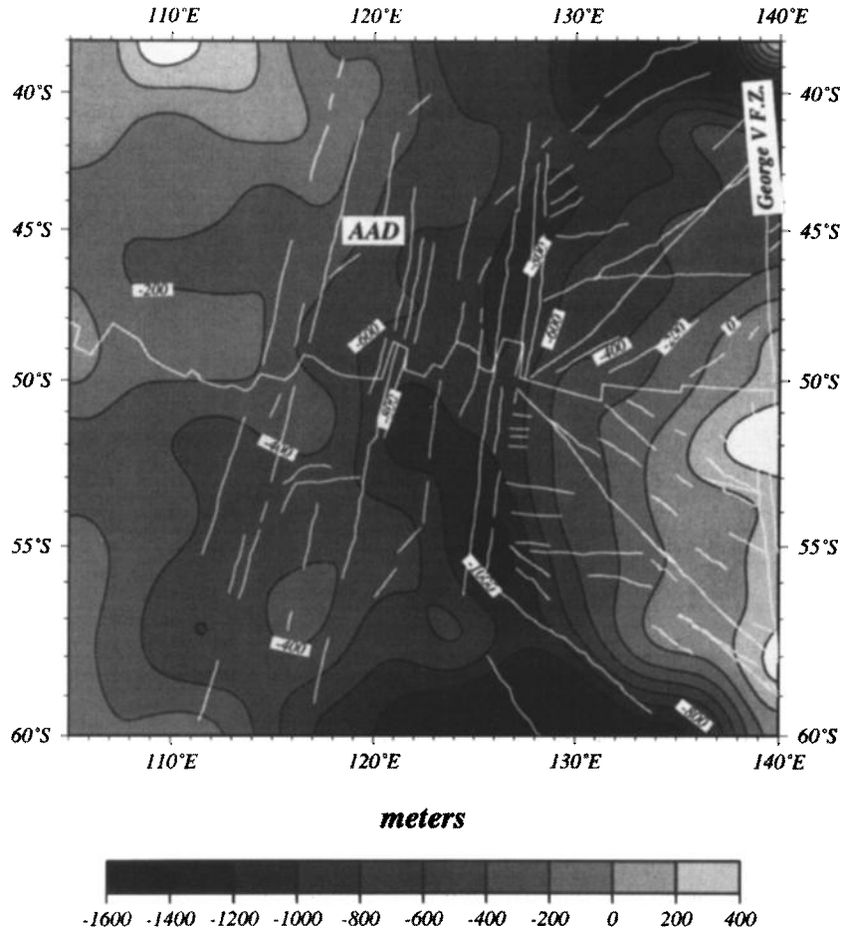

Figure 4. The AAD's residual depth anomaly [*Marks et al.*, 1991]. The AAD is associated with a residual depth anomaly that extends NNE and SSE across the Australian and Antarctic plates, respectively, to the continental margins. The broad, west facing, V shape of the depth anomaly suggests a slow westward migration at 15-25 mm yr^{-1} [*Marks et al.*, 1990] over the last 30 Myr, and about 30 mm yr^{-1} prior to its intersection with the eastern bounding transform fault of the AAD. Overlaid in white are lineations derived from satellite gravity anomaly data [*Smith and Sandwell*, 1995]. In addition to north-south trending transform faults, multiple lineations define westward pointing, V-shaped structures that reflect past episodes of rift propagation east of the AAD.

Asthenospheric flow toward the AAD has also been suggested based on episodes of ridge propagation observed on the SEIR [*Vogt et al.*, 1984; *Marks et al.*, 1990, 1991; *Sempéré et al.*, 1996, 1997]. Oblique topographic lineations off axis, extending both east and west of the AAD, have been identified with satellite gravity data [*Phipps Morgan and Sandwell*, 1994]. The most prominent of the off-axis lineations are associated with large propagating rifts that converge on the AAD from both the east and the west on the SEIR [*Phipps Morgan and Sandwell*, 1994; *Sempéré et al.*, 1996, 1997]. Many of the off-axis lineations and oblique structures terminate at the eastern bounding transform of the AAD near the 25 Ma isochron, consistent with the age of the development of the rough gravity and bathymetric signature of this region (Figures 3 and 4). The George V ridge transform system (~139°E) appears to have been the locus of origin for many of the propagating ridges on the SEIR east of the AAD (Figure 4). Off-axis traces of these propagating ridges indicate a propagation rate of 30-45 mm yr^{-1} toward the AAD. Although the cause of rift propagation is poorly understood, these propagation rates can be interpreted as the flow velocity of the asthenospheric flow within the melt column (*Vogt et al.*, [1984], *Marks et al.* [1990, 1991], *Sempéré et al.* [1996], also see discussion) and are similar to the flow velocity inferred from the migration of the Indian-Pacific isotopic boundary [*Pyle et al.*, 1995] (Figure 3).

Method

We study passive and buoyant asthenospheric flow due to continental separation in a constant- and variable-viscosity upper mantle using a three-dimensional, finite-volume formulation of viscous fluid flow based on the Semi-Implicit Method for Pressure-Linked Equations ShorTened (SIMPLEST) algorithm [*Patankar*, 1980]. In order to make the problem tractable, we approximate the separation of the Australia and Antarctica continents by diverging blocks in constant- and variable-viscosity mediums along a four-segment rift, representing the SEIR (Figure 5). Our models do not incorporate the complex process of continental rifting and thus cannot be taken as representative of the flow pattern immediately after continental separation (100-45 Ma). Our

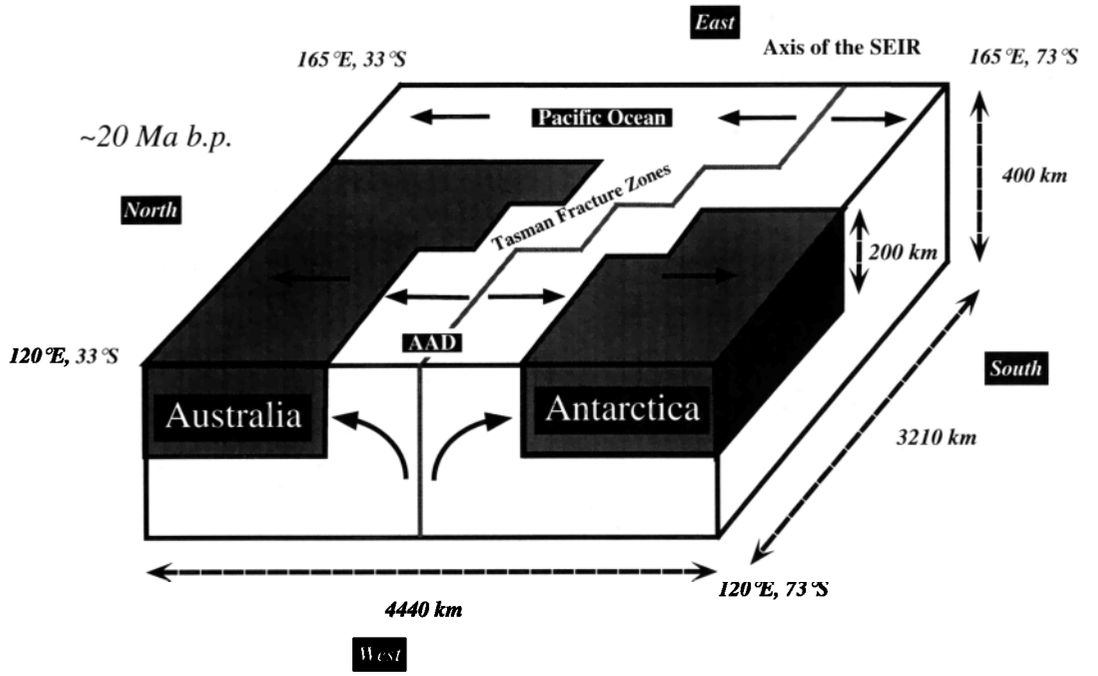

Figure 5. Schematic of the model geometry. The lengths and ridge segmentation are chosen to approximate the configuration of the Southern Ocean (Figure 1); our model segmentation is representative of the gross segmentation patterns of the SEIR over the last 40 Myr, including the Tasman fracture zone complex. Our model extends from the AAD at ~120° E, through the South Tasman Rise to 165°E. In this Cartesian model, 1 km in model latitude is assumed to equal 0.64 km in model longitude, the approximate relationship at 50° S.

geometry also neglects possible effects the Pacific subduction zone associated with the Macquarie Ridge may have on upper mantle circulation on this region [*Baumgardner,* 1988]. The focus of our study, however, is the first-order upper mantle flow structure beneath the SEIR within the last 40 Myr between 120°E and 136°E. We assume that the AAD at 120°E is an axis of symmetry and model only the eastern half of the Southern Ocean. Our rectangular numerical domain, scaled to the present ocean basin, extends 3210 km from east to west, 4400 km from north to south, and 400 km in depth and is divided into a regular grid consisting of 25 x 28 x 25 control volumes.

Governing Equations

The equations for Newtonian, incompressible convection solved by our algorithm are the equations of continuity, momentum, energy, and conservation of a passive tracer:

$$\nabla \bullet \mathbf{u} = 0 \tag{1}$$

$$\nabla P' = \nabla \bullet (\mu \nabla \mathbf{u}) + \rho \alpha_v (T - T_o)\mathbf{g} \tag{2}$$

$$\frac{\partial T}{\partial t} + \mathbf{u} \bullet \nabla T = \kappa \nabla^2 T \tag{3}$$

$$\frac{\partial \delta}{\partial t} + \mathbf{u} \bullet \nabla \delta = 0 \tag{4}$$

where $\mathbf{u}$ is the velocity vector, T is the temperature, P' is the dynamic pressure, $\mathbf{g}$ is the gravitational acceleration, ρ is the mantle density (3330 kg m^{-3}), α_v is the volumetric expansion coefficient (3×10^{-5} °C^{-1}), T_o is the reference temperature (1350°C), κ is the thermal diffusivity (10^{-6} m^2 s^{-1}), μ is the viscosity, and δ is a tracer with a numerical value of either 1 or 0 assigned to the Indian and Pacific mantle reservoirs, respectively. In passive flow simulations, in which buoyancy is neglected, the second term on the right-hand side of (2) is dropped. Equations of the form of (4), in which the associated Peclet number approaches infinity, are associated with numerical diffusion when flow is oblique to control volume faces [*Patankar,* 1980]. In our models, we have attempted to minimize numerical diffusion by orienting the grid lines orthogonal to the predominant flow in the region of interest and by employing a second-order upwind differencing method [*Spalding,* 1979, 1980].

Boundary Conditions

In all simulations, the continents are modeled as regions of prescribed velocities, corresponding to the half spreading rate of the system, 37 mm yr^{-1}. The continents extend from the western end of the domain to approximately halfway along strike of the ridge axis, beyond the model Tasman Fracture Zone Complex, and extend to a depth of 200 km (Figure 5). The internal regions of the continents are held at a fixed temperature of 1000°C below 50 km, decreasing to 0°C at the surface according to an error function relationship. These conditions mimic the expected thermal conditions of Cretaceous cratons [*Guillou and Jaupart,* 1995]. Where continents intersect the model boundaries, the continental pressure and temperature conditions always override the boundary conditions ascribed elsewhere.

In passive flow models, the northern, southern, and bottom boundaries of the numerical domain are assigned a pressure condition corresponding to a dynamic pressure of 0.0 (e.g., (2)). This combination of velocity and pressure boundary conditions can approximate the analytic, passive corner flow solutions of *Reid and Jackson* [1981] and *Batchelor* [1967] without artificially forcing flow at the bottom boundary. In models including buoyancy forces, only the bottom boundary is assigned a dynamic pressure of 0.0 and the northern and southern boundaries are assigned velocities derived from the passive flow solution. The top surface is assigned a constant velocity on either side of the rift of 37 mm yr^{-1}, the average half spreading rate of the SEIR within the AAD at the present time [*Palmer et al.*, 1993]. Material is allowed to pass through all but the top, eastern, and western boundaries. The western and eastern boundaries of the model are assumed to be symmetry planes through which no flux of material is allowed.

Temperature boundary conditions are applied as flux conditions to (3) such that the top surface, corresponding to the seafloor, is maintained at a temperature of 0°C. All side boundaries are assumed adiabatic. The bottom thermal boundary condition is also adiabatic with only incoming material having a prescribed temperature [*Spalding*, 1979, 1980]. Thus the temperature at this boundary is not "fixed," resulting in a more natural way of specifying temperatures on an artificial boundary within a larger convecting system [*Spalding*, 1980]. In simulations without an along-axis temperature anomaly, material passing into the numerical domain through the bottom is assigned a temperature of 1400°C. In simulations with temperature anomalies beneath the AAD, cooler than normal upper mantle temperatures are prescribed by linearly decreasing the influx temperature from 1400°C at 145°E to a lower value at 120°E. This results in a maximum temperature anomaly centered beneath the AAD at 120°E, as described by *Kuo et al.* [1996] (Figure 1), and a linear temperature gradient along the SEIR.

Rheology

In variable viscosity simulations, the viscosity of the mantle is defined by an exponential relationship dependent on both lithostatic pressure P (assumed to be a linear function of depth) and temperature:

$$\mu[T,P(z)] = \mu_o \exp\left\{\frac{\left[\frac{E+P(z)V}{RT}\right]}{\left[\frac{E+P_oV}{RT_o}\right]}\right\}, \quad (5)$$

where R is the universal gas constant (J mol^{-1} K^{-1}). We have adopted values of activation volume, V=10^{-5} m^3 mol^{-1}, and activation energy, E=520 kJ mol^{-1}, that match average laboratory-determined values of an anhydrous olivine/pyroxene composition [*Goetz*, 1978; *Cooper and Kohlsted*, 1986]. This combination of parameters produces an order of magnitude change in viscosity over a temperature interval of approximately 125°C at constant pressure. Owing to the pressure dependency of our viscosity relationship, a twentyfold viscosity increase occurs over a pressure interval equal to a depth increase of ~100 km. In passive flow simulations the choice of reference viscosity μ_0 is immaterial since only the contrasts in velocity affect the solution. However, solutions involving buoyancy forces are sensitive to both the absolute level of the mean viscosity and contrasts in viscosity. Thus we explore solutions with reference viscosities of 10^{19}-10^{21} Pa s, a range that spans current estimates of oceanic upper mantle viscosities [*Cathles*, 1975; *Turcotte and Schubert*, 1982]. To preserve numerical stability, viscosities within our numerical domain are limited to a minimum and maximum values of $0.005\mu_0$ and $1000\mu_0$, respectively, thus limiting the total variation in viscosity within our models to about 5 orders of magnitude [*Patankar*, 1980; *Ogawa et al.*, 1991].

Initial Conditions

At 40 Ma all noncontinental material west of approximately 142°E is assigned to be an Indian type, while material east of this boundary is assigned to be Pacific. This is in accordance with our current understanding of the distribution of mantle sources at that time [*Pyle et al.*, 1995, *Lanyon et al.*, 1995]. Throughout the simulation, material entering the bottom of the numerical domain west of the 142°E boundary is assigned to be Indian, while material entering to the east is assigned to be Pacific.

At the start of each simulation, the continents are separated by 500 km to approximate their configuration at 40 Ma. The initial temperature conditions for all simulations are those for the passive spreading solution to the model ridge geometry and a spreading rate of 37 mm yr^{-1} but without the complicating factors of continents or along-axis temperature anomalies. In all solutions flow is allowed to develop in the numerical domain over a dimensional time of 40 Myr. Each time step covers 5 Myr and contains 3000 iterations on the flow equations. This ensures convergence to a stable velocity, pressure, and temperature solution that satisfies the velocities and temperatures imposed in the continents. The faces of the continents within the numerical box effectively act as boundary conditions for an expanding solution domain that corresponds to the upper mantle of the opening Southern Ocean.

Benchmarks of the Finite-Volume Algorithm

To ensure that our numerical algorithm is applicable to mantle flow problems, we benchmarked our finite-volume implementation against results of analytic corner flow [*Batchelor*, 1967], and published constant-viscosity, three-dimensional corner flow [*Phipps Morgan and Forsyth*, 1988], two-dimensional variable-viscosity corner flow solutions that we obtained with the algorithm *ConMan* [*King et al.*, 1989], and the constant- and variable-viscosity natural convection benchmarks outlined by *Blankenbach et al.* [1989]. For constant- and variable- viscosity corner flow tests, our algorithm reproduced velocity and temperature fields well. For natural convection benchmarks in a constant viscosity medium, we obtained solutions also within the range of published values [*Blankenbach et al.*, 1989]. However, for natural convection benchmarks with temperature-dependent viscosity our Nusselt numbers and root-mean-square velocities are in error by about 10% of published values.

Previous work has shown that the poor convective solutions obtained using the SIMPLEST algorithm for temperature-dependent viscosities are a result of the staggered nature of the grid in which the fluid viscosity is defined at the cell centers while velocities are obtained on the cell walls [*Ogawa et al.*, 1991]. The harmonic mean interpolation

scheme, which is used to extrapolate viscosities to the cell edges, results in significant errors when there is a component of flow perpendicular to steep viscosity gradients. Thus, in the variable viscosity convection solutions, the algorithm is inaccurate in regions where material enters and exits the thermal boundary layers. We have not implemented a more sophisticated viscosity interpolation scheme to minimize these errors for two reasons. First, in our models non-dimensionalized flow-parallel viscosity gradients are much smaller than in the convection benchmarks. Second, numerical errors of about 10% within our solutions are acceptable, given the other simplifications and approximations that are incorporated into our regional model. In our simulations, it is not our intention to model small-scale complexity in the flow and temperature fields beneath the ridge axis but, rather, to define the large-scale flow features of the upper mantle.

Results of Calculations

Passive Flow in a Constant Viscosity Upper Mantle

Figure 6 shows the results of our calculations in a constant-viscosity mantle. Initially, between 40 and 30 Ma, a significant component of along-axis flow develops (>15 mm yr^{-1}) to fill in the narrow gap between the diverging continents. At this time, enhanced subaxial upwelling is also present between 120°E and 145°E since flow is focused into the narrow region between the continents. In this constant viscosity simulation, Tasmania acts as an impediment to along-axis flow that would otherwise come directly from the Pacific and forces the horizontal flow to originate from the south and east in early time steps. After 30 Ma, the increased upwelling and longitudinal flow diminishes. The flow associated with the ridge between 120°E and 135°E is symmetric about the ridge axis and approximates the corner flow solution [*Reid and Jackson,* 1981; *Batchelor,* 1967], while the flow beneath the ridge-transform-ridge (RTR) intersections between 135°E and 150°E is similar in structure to the flow solutions of *Phipps Morgan and Forsyth* [1988] and *Rabinowicz et al.* [1993] for RTR geometries. The ridge-transform geometry we employ to model the complex Tasman transform zone distributes the associated mantle flow perturbation over a geographic range of ~1000 km (Figure 6), and the combined effects of the RTR intersections and continents result in a general counterclockwise perturbation of the flow field. Flow into the wake of the diverging continents migrates from the south and east, through the large transforms associated with the Tasman fracture zone complex.

In all simulations we track the composition of material within our domain using (4). To predict the volcanic (surface) expression of the Indian-Pacific isotopic boundary, we plot the maximum westward displacement of the boundary at the axis on the seafloor for a given time step. This parcel of seafloor then moves off-axis as part of the lithosphere. Thus the predicted isotopic boundary on off axis seafloor is the maximum westward displacement of Pacific mantle beneath the ridge axis at the time the seafloor formed. This predicts the surface expression of the isotopic boundary that would be observed by off-axis dredging or drilling. For the constant viscosity simulation, this calculation demonstrates that the along-axis flow present is insufficient to advect the Indian-Pacific isotopic boundary from its initial position within the Tasman transform complex to its present axial location within the AAD (Figure 6).

To compare our solutions with the along-axis flow velocities inferred from the traces of propagating rifts, we also calculate the horizontal trace of a particle that is initially at the George V fracture zone 25 Ma and that is confined in the subaxial melting region at a depth of ~50 km. Thus we assume that propagating rifts are tied to melting anomalies which are advected along axis. As for the isotopic boundary, the calculated propagating ridge trace does not match inferred along-axis flow velocities (Figure 6). The trace migrates in Figure 6 with an average velocity of only 12 mm yr^{-1} compared to the observed propagating rift velocities of 30-45 mm yr^{-1}. These calculations demonstrate the need for more a complex model parameterization to match the geophysical and geochemical evidence for more extensive along-axis flow beneath the SEIR.

Passive Flow in a Variable Viscosity Upper Mantle

Our first variable viscosity simulation included separation of the Australian and Antarctic continents in a temperature- and pressure-dependent viscosity mantle (equation (5)) with a constant bottom influx temperature. The results (Figure 7) are significantly different from the constant viscosity simulation. In contrast to the constant viscosity calculations, large-scale (~1000 km) distributed flow perturbations are not associated with the Tasman transform fault complex (Figure 7). The RTR-induced flow is of a lower magnitude than in the constant viscosity simulations and is localized to within ~150 km of the RTR intersections. In addition, a "channel" of low viscosities exists beneath the ridge axis, extending through the transform complex and linking the model Indian and Pacific Ocean basins. Higher off-axis viscosities focus along-axis flow beneath the ridge axis and impede the off-axis development of the large-scale counterclockwise circulation observed in the constant viscosity calculations.

In variable viscosity calculations, mantle viscosities are high beneath the continents owing to both the depth dependence of (5) and the cooler mantle temperatures that result from holding the deeper portions of continents at 1000°C. The viscosity structure couples the continents to the underlying lower mantle regions effectively increasing the continental root (section b-b' in Figure 7). This coupling enhances upwelling and reduces the along-axis flow necessary to satisfy continuity between the diverging continents (subcontinental regions in section b-b' of Figure 7). This effect also results in a lower propagating ridge velocity (Figure 7) compared with those shown in Figure 6. In variable-viscosity calculations which do not fix the continental temperature (that is, the thermal structure within the continent varies proportionally to the square root of distance away from the ridge axis), along-axis flow velocities are initially ~40% higher than those presented in Figure 7.

As in the constant viscosity simulation, the flow field due to continental separation in a variable-viscosity upper mantle does not advect model Indian-Pacific isotope boundary from its initial location just west of Tasmania to a position within the AAD (Figure 7). The boundary migrates only about 100 km along axis. Additionally, the trace of the simulated propagating ridge migrates at only about 5 mm yr^{-1}, an order

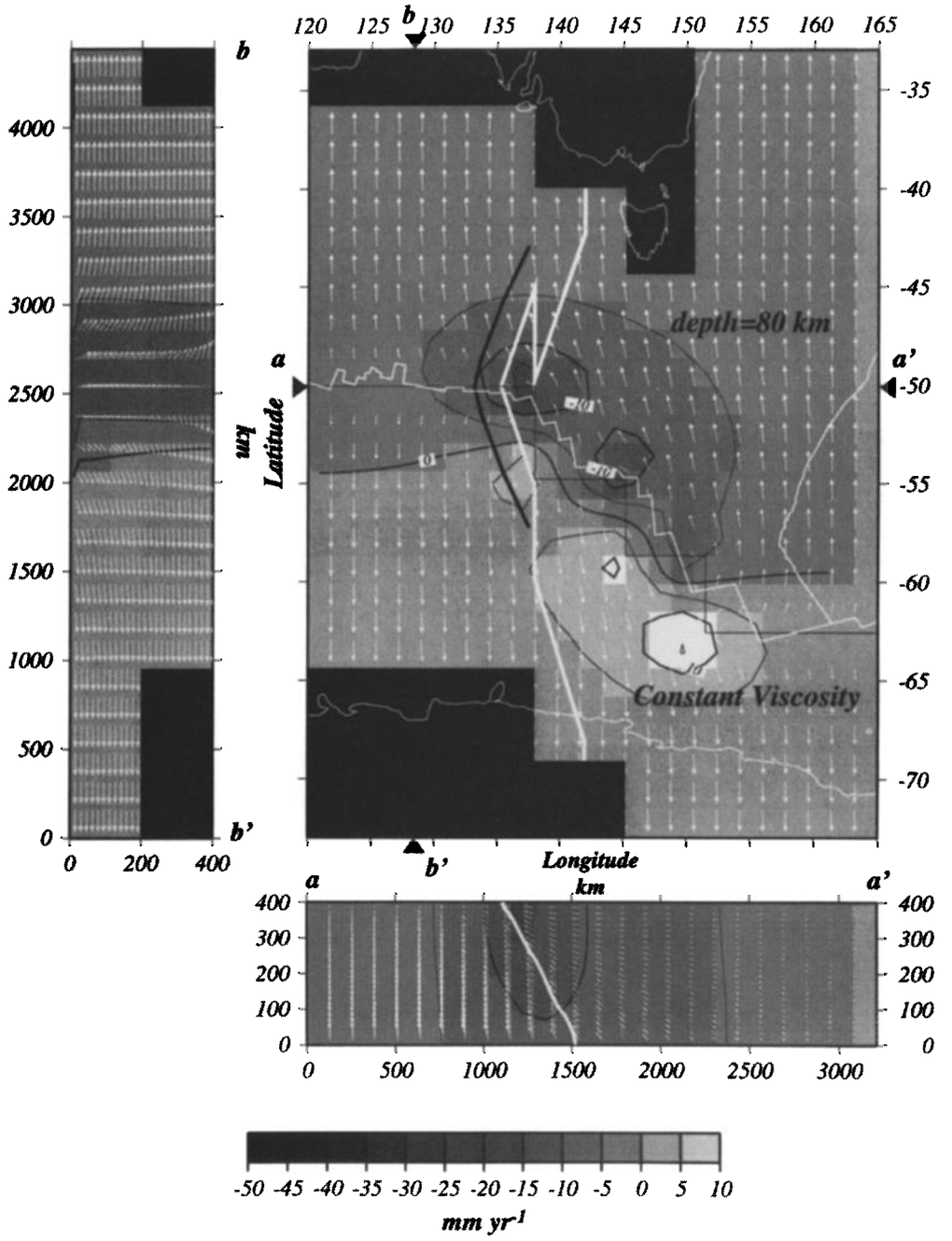

Figure 6. Planform of present-day passive flow in a constant-viscosity mantle due to separation of the Australian and Antarctic continents in a constant viscosity mantle. This and subsequent figures are arranged as follows: (center) a horizontal plane at a depth of 80 km which approximates the base of the melt column. (bottom), (labeled a-a'), a vertical slice beneath the axis of the SEIR between 120°E and 136°E and extending along strike to the east through older lithosphere created on the SEIR east of the Tasman fracture zones, and (left), (labeled b-b'), a vertical cross section perpendicular to the axis at approximately 128°E. White vectors represent calculated mantle flow patterns. The thick white line in the center represents the surface (volcanic) expression of the Indian-Pacific isotopic boundary (see text), while at bottom, the white line represents the boundary throughout the mantle. A calculated propagating rift trajectory (see text) is shown by the solid black line. The position of the continents is shown by black blocks. The current locations of the Australian and Antarctic continents are traced in white for comparison. The model ridge axis is indicated by a solid line, and the observed ridge axis in this coordinate system is traced in white. The center is annotated and marked in geographic coordinates, while cross sections a-a' and b-b' are annotated in equivalent kilometers. Note that at high latitudes, the geographic location of the Antarctic continent plots well beyond the model location owing to the distortion that our Cartesian model geometry introduces in this region.

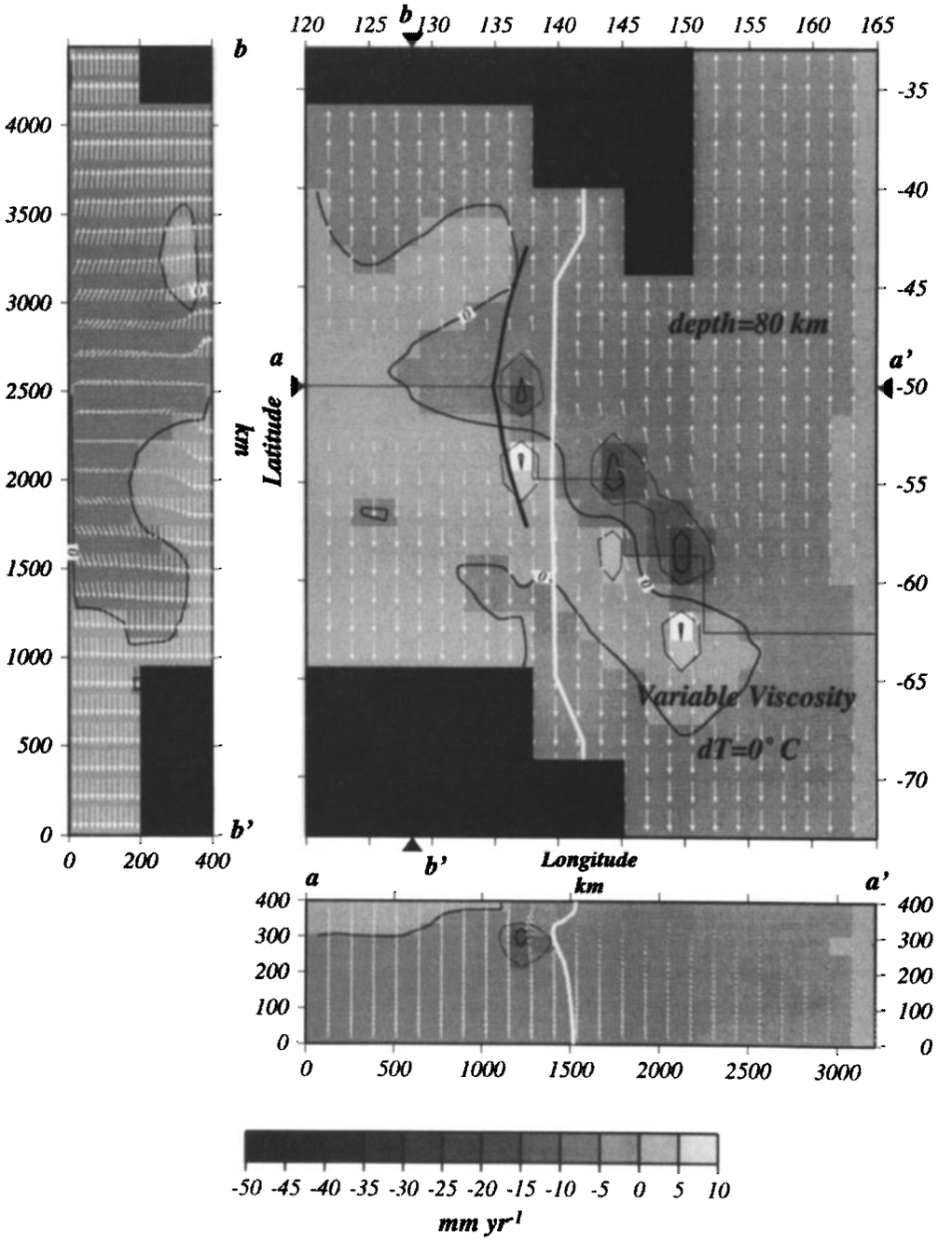

Figure 7. Planform of present-day passive upper mantle flow due to the separation of the Australian and Antarctic continents in a mantle with a temperature- and pressure-dependent viscosity. The influx temperature on the bottom boundary in this simulation is constant. In contrast to flow in a constant viscosity mantle, little axis-parallel flow occurs off axis owing to the focusing effects of the low-viscosity zone beneath the ridge axis. The high angle that the model propagating ridge trace intersects the ridge axis (~70°) indicates an along-axis flow component of about 5 mm yr^{-1}, lower than that inferred from ridge traces shown in Figure 4.

of magnitude more slowly than the velocity inferred from Figure 4. These results again demonstrate that further complexities in the model parameters are required to reproduce the inferred magnitude of along-axis flow.

Passive Flow in a Variable Viscosity Upper Mantle With Temperature Gradients

Figures 8 and 9 show a solution for passive flow in a variable-viscosity upper mantle with a linear temperature gradient. In this solution, the temperature of the mantle upwelling through the lower boundary is 300°C cooler beneath the AAD than "normal" upwelling mantle east of 145° E. The introduction of temperature anomalies beneath the ridge results in the development of sustained along-axis flow toward regions of cooler mantle (Figure 8). Owing to lower mantle temperatures, a wedge of high viscosities exists beneath the ridge axis of the AAD (Figure 9, section a-a' and Figure 10). A higher-viscosity mantle at depth is more difficult to upwell, and thus along-axis flow in the low-viscosity region beneath

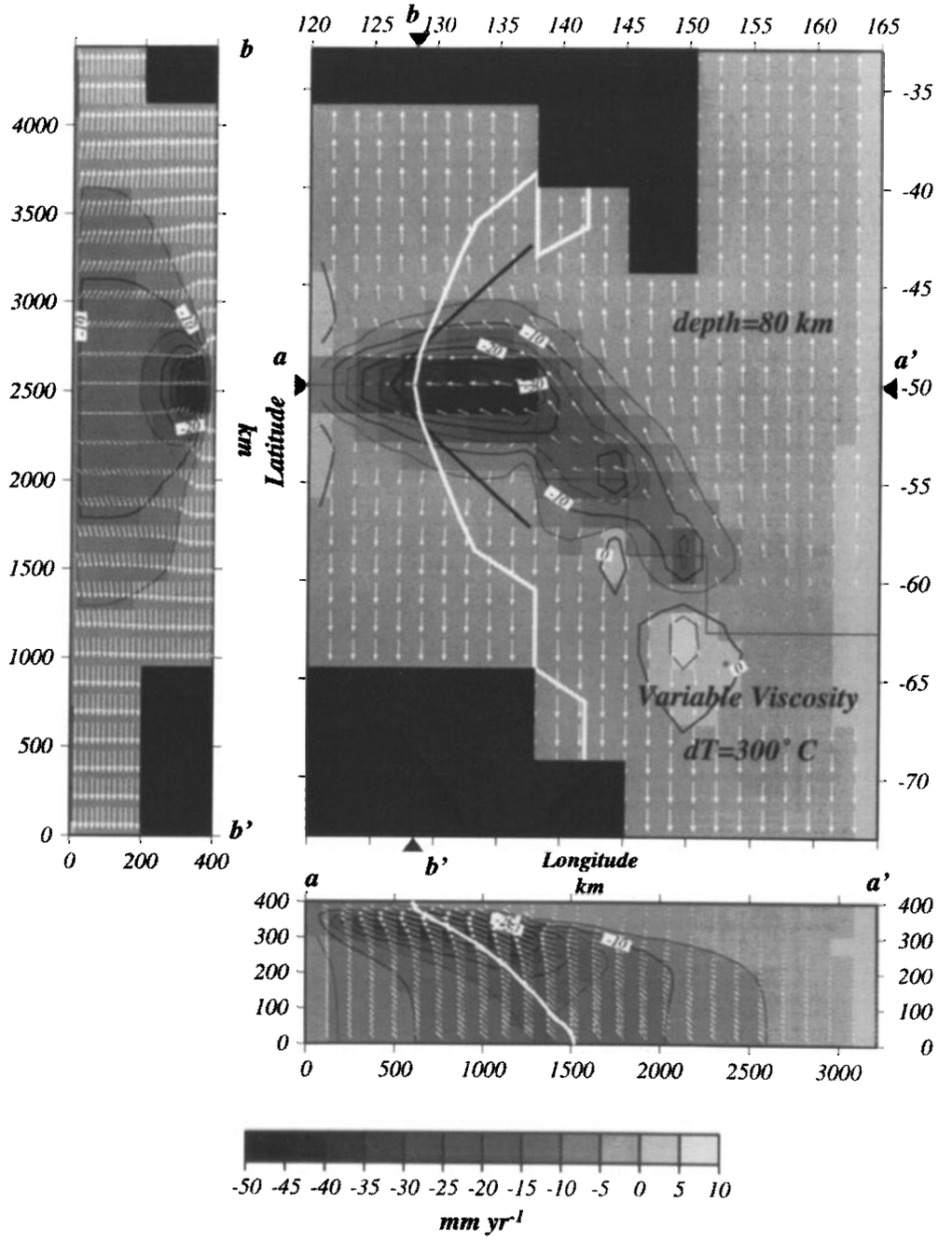

Figure 8. Planform of present-day passive upper mantle flow due to the separation of the Australian and Antarctic continents in a mantle with a temperature- and pressure-dependent viscosity and a horizontal basal temperature gradient. In this simulation, the influx temperature decreases linearly from 1400°C at 145°E to 1100°C at 120°E. Significant along-strike flow develops and continues to the present day owing to higher mantle viscosities beneath the AAD. The along-strike flow is concentrated beneath the ridge axis in the subaxial, low-viscosity region. The transform fault complex acts as a channel through which the along-axis flow is able to migrate without significant hindrance. The model-propagating ridge trace intersects the ridge axis at an angle similar to that shown in Figure 4, and the final along-axis position of the isotopic boundary is consistent with the observed location (Figure 3). Note that the propagating rift trace and the migrating isotopic boundary cross since the propagating rift marker is required to remain at a depth of 50 km beneath the ridge axis, while the isotopic boundary is advected by the full, three-dimensional flow field.

the ridge axis develops to fill the gap left by the separating continents. This flow results in the advection of warmer asthenosphere into the low viscosity region overlying cooler, deeper mantle regions (Figure 10, bottom). This flow subdues the deeper horizontal temperature gradient and results in a vertical temperature inversion in the subaxial mantle (Figure 10, bottom).

In Figure 8, the along-axis flow velocity inferred from the off-axis trace of the model propagating rift is about 35 mm yr^{-1} between 125° and 140°E. Figure 11 shows the mean

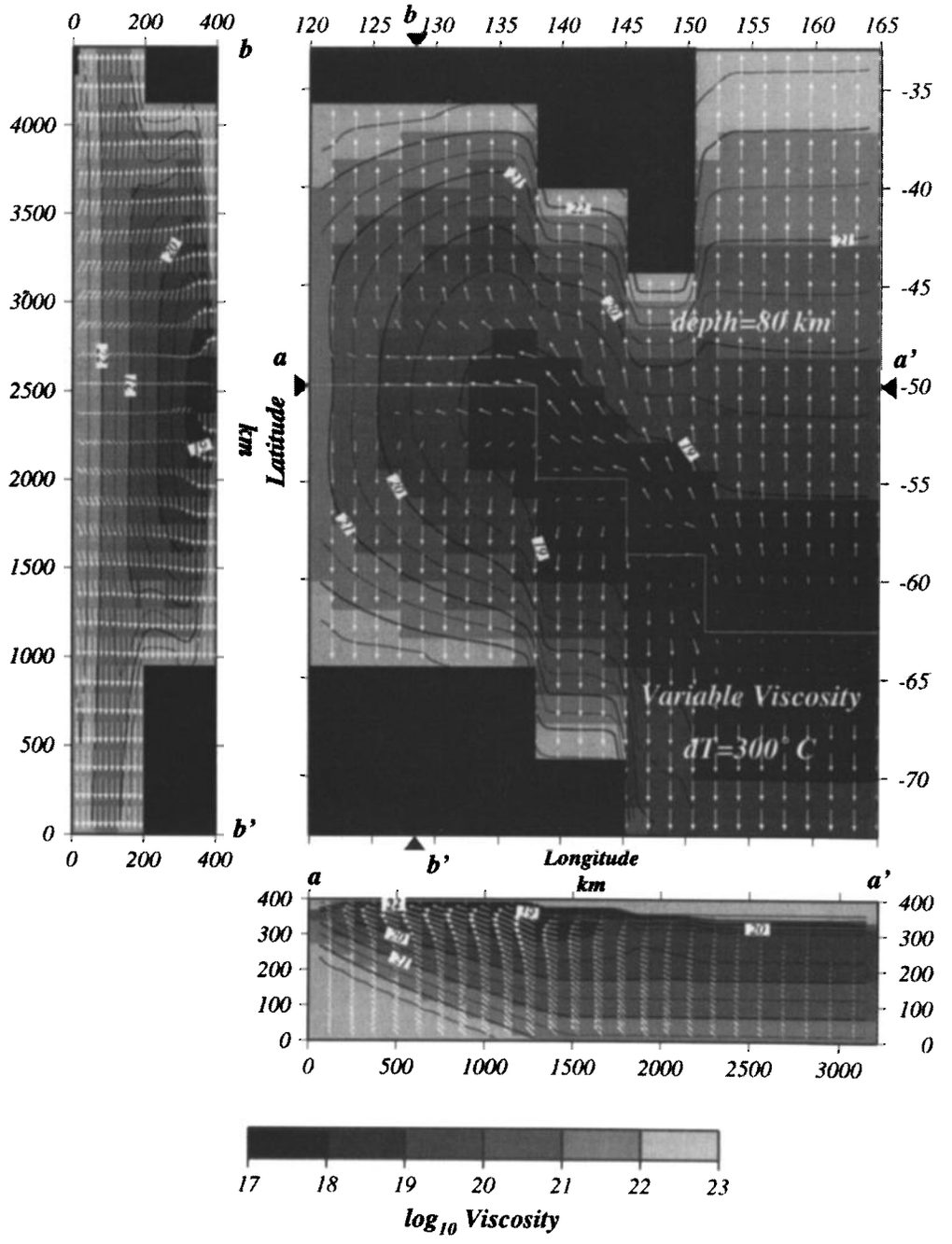

Figure 9. Viscosity structure with superimposed flow vectors for the solution shown in Figure 8. Average mantle viscosity increases toward the AAD owing to the presence of cooler upper mantle, although a viscosity minimum remains centered beneath the ridge axis at a depth of 50-100 km. The general viscosity structure resembles a wedge of low viscosities as the AAD is approached along-strike from the east.

along-axis flow velocity at 50 km depth as a function of the temperature anomaly beneath the AAD. The predicted along-axis flow velocity for a 300°C temperature anomaly is in reasonable agreement with velocities inferred from the off-axis propagating ridge traces shown in Figure 4. Figure 12 shows the predicted present-day, axial location of the Indian-Pacific isotopic boundary as a function of mantle temperature anomaly. Again, a mantle temperature anomaly of about 300°C is required to advect Pacific mantle to its current location in the AAD. This temperature anomaly is significantly greater than the anomaly estimated by other geochemical and geophysical data, a result which suggests that buoyancy forces play a significant role.

Buoyancy in a Variable Viscosity Upper Mantle With Temperature Gradients

A solution for a model involving buoyancy is presented in Figures 13 and 14. In this example, the temperature anomaly beneath the AAD is 150°C and the reference upper mantle viscosity at 200 km and 1350°C is 10^{20} Pa s. Flow in the buoyant simulation is similar to that shown in a passive

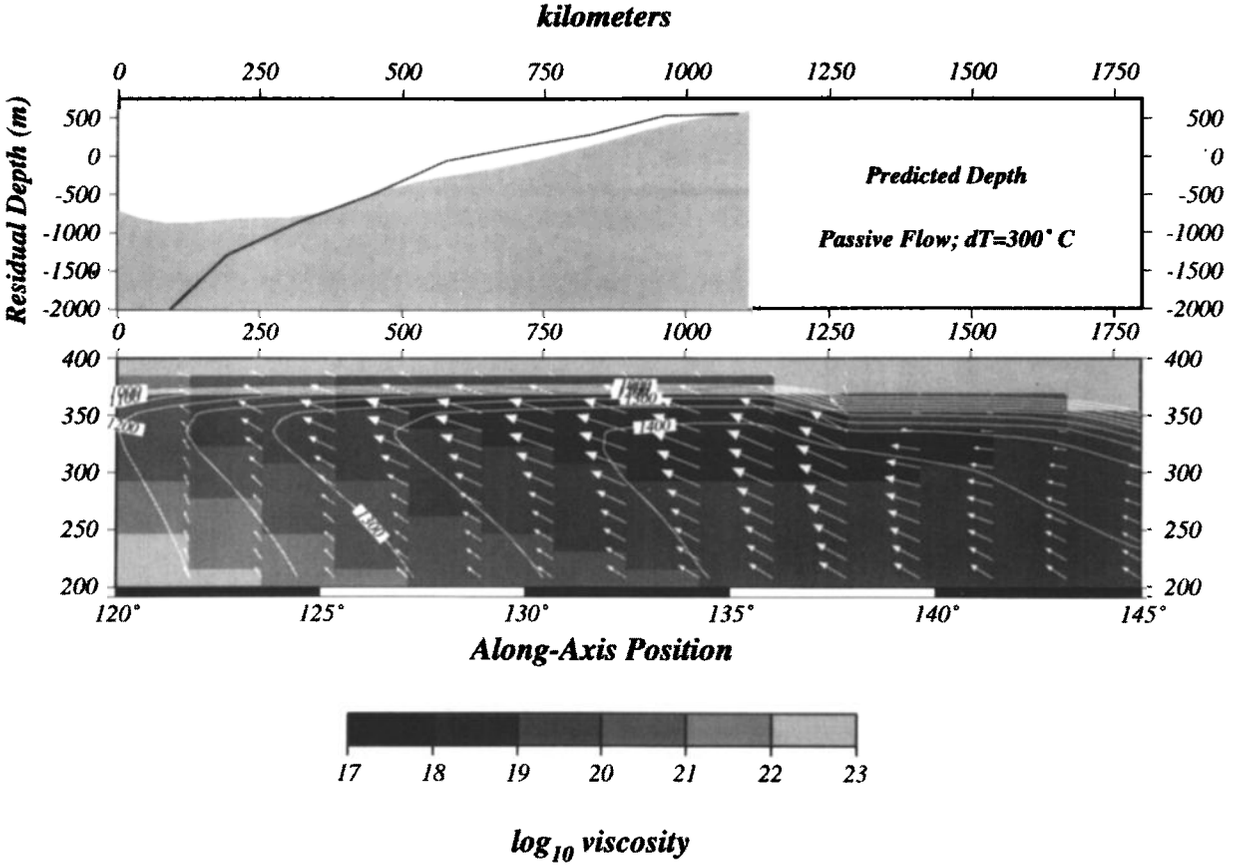

Figure 10. (top) Along-strike depth variation calculated from this model (see text), including static (thermal), dynamic (pressure), and isostatic components assuming a compensation depth of 125 km (solid line), and the observed residual depth anomaly (shaded area) [*Marks et al.*, 1991]. (bottom) Vertical along-axis section for the solution shown in Figures 8 and 9, including the SEIR between 120°E and 136°E. White contours show temperature variations averaged within the two cells neighboring the ridge axis on either flank (minimum contoured temperature value is 1000°C). White vectors indicate calculated mantle flow patterns directly beneath the ridge axis; the average viscosity structure beneath the ridge axis is shown by shaded contours. Significant along-axis flow develops owing to the presence of a cool, higher-viscosity region beneath the AAD. Flow magnitudes in the low-viscosity region are nearly twice the spreading rate because both vertical and along-axis flow components exist. The subaxial flow also results in the advection of warmer mantle on top of cooler, higher-viscosity mantle deeper within the mantle and produces a significantly different thermal structure than would be expected from simple two-dimensional, vertical flow. The process subdues shallow temperature anomalies and results in a temperature inversion in the subaxial asthenosphere.

solution with a 300°C temperature anomaly (Figures 8 and 9); reduced upwelling beneath the AAD draws material through the low-viscosity channel beneath the ridge axis. The addition of buoyancy forces into our calculations significantly lessens the temperature anomaly required to match our constraints. Buoyancy forces tend to inhibit the upwelling of cooler mantle beneath the AAD. A temperature anomaly of about 100-200°C can match the inferred propagating ridge velocities (Figure 11) and the final predicted position of the isotope boundary (Figure 12). The thermal anomaly required depends on the reference upper mantle viscosity used; increasing μ_o increases the required temperature anomaly because buoyancy forces become less important. This effect can be seen directly in the plots of the along-axis flow velocity against temperature anomaly (Figure 11).

As in the passive flow simulation (Figure 10, bottom), high viscosities at depth beneath the AAD facilitate along-axis advection of warmer asthenosphere above cooler regions and produce a vertical temperature inversion in the subaxial mantle (Figure 14, bottom). However, for a given along-axis flow velocity, the wedge of high viscosities below the AAD is not as pronounced as in the simulations without buoyancy because the required horizontal temperature gradient is smaller.

Predicted Residual Depths

Our solutions can also be used to estimate the along-strike residual depth using the relationship

$$w(x) = \alpha_v \int_{d_c}^{o} [T(x,z) - 1400°\mathrm{C}]dz + \frac{[P'(x,0) - P'_o]}{(\rho_m - \rho_w)g} + \left[1 + \frac{(\rho_o - \rho_w)}{(\rho_m - \rho_o)}\right]^{-1} \psi[1400°C - T_{80}(x)] + d_o \quad (6)$$

where P'_o is the maximum surface dynamic pressure value

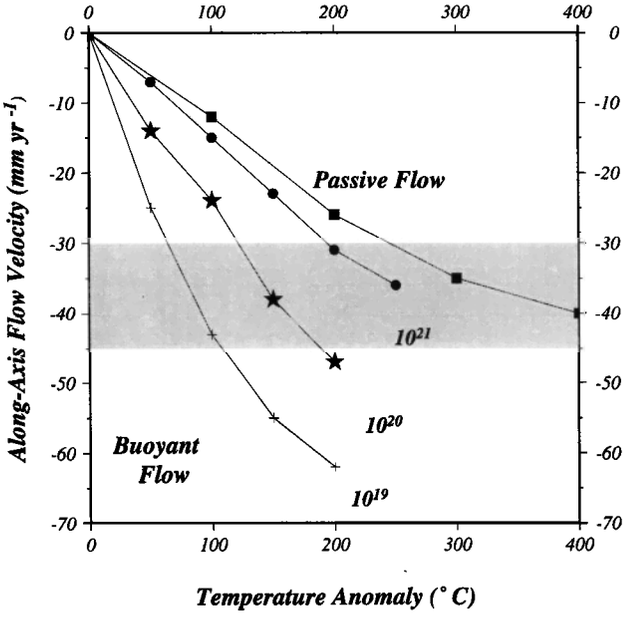

Figure 11. The mean along-axis flow velocity beneath the SEIR at a depth of 50 km between 125° and ~137°E as a function of temperature anomaly beneath the AAD. Passive flow results are shown by squares, and buoyant results are shown by the circles, stars, and crosses. Buoyant results are for values of the reference upper mantle viscosity μ_o spanning 2 orders of magnitude (10^{19}-10^{21} Pa s). Shaded area between -30 and -45 mm yr^{-1} outlines the acceptable range of along-axis flow velocities inferred from the off-axis traces of propagating ridges (Figure 4).

along the ridge axis (only pressure differences are important for this calculation), d_c is the compensation depth, ρ_c is the density of the crust (2730 kg m^{-3}), ρ_w is the density of water (1030 kg m^{-3}), ρ_m is the mantle density (3330 kg m^{-3}), ψ is the rate of change of the crustal thickness with the mantle temperature at the base of the melt column (assumed to be 80 km) (ψ=km °C^{-1}), and d_o is a depth chosen such that the predicted and observed residual depths are equal at the George V fracture zone (Figure 4). In this equation, the first term on the right-hand side represents thermal topography, the second accounts for 'hydraulic head' equivalent topography, and the third term accounts for the isostatic adjustment in depth with crustal thickness (derived from the mantle temperature at a depth of 80 km). We assume a compensation depth of 125 km [*Forsyth,* 1992] and a value of ψ=0.04 km °C^{-1}, which falls near the center of the range of current estimates [*McKenzie,* 1984; *Klein and Langmuir,* 1987; *Su et al.,* 1994; *West et al.,* 1994].

The predicted and observed residual depths for the passive flow solution with a temperature anomaly of 300°C and the buoyant flow solution with a temperature anomaly of 150°C and μ_o=10^{20} Pa s are shown in Figures 10 (top) and 14 (top), respectively. For the passive flow solution (Figure 10), the predicted regional depth variation overestimates the observed depth variation by about 1 km (Figure 10). Because warmer material is advected toward the AAD within the low-viscosity zone, a 300°C temperature anomaly at depth results in a mantle temperature variation of about 200°C within the melt zone. For a value of ψ=0.04 km °C^{-1}, a ~200°C temperature anomaly within the melting region results in an 8 km variation in crustal thickness. This estimate is inconsistent with predicted and observed crustal thickness variation of 3-4 km between the AAD and the SEIR to the east [*West et al.,* 1994, also manuscript in preparation, 1997; *Tolstoy et al.,* 1995].

For the buoyant flow solution (Figure 14, upper panel), the predicted and observed maximum regional variations match reasonably well. The 150°C temperature anomaly results in a horizontal temperature variation of about 75°C in the melting region and an estimated crustal thickness variation of about 3 km. This is more compatible with current estimates of crustal thickness variation in this region [*West et al.,* 1994, also manuscript in preparation, 1997; *Tolstoy et al.,* 1995]. These results demonstrate that a temperature anomaly of 100 - 200°C at a depth of 400 km can match along-axis variations in seafloor depth and crustal thickness as well as the constraints on along-axis flow velocities.

Discussion

Our models and results address questions first raised by *Alvarez* [1982, 1990] and refine the results of *Parmentier and Oliver* [1979] and *Kuo et al.* [1995]. We have established the first-order structure of asthenospheric flow resulting from the separation of the Australian and Antarctic continents in an effort to reproduce inferred along-axis mantle flow velocities,

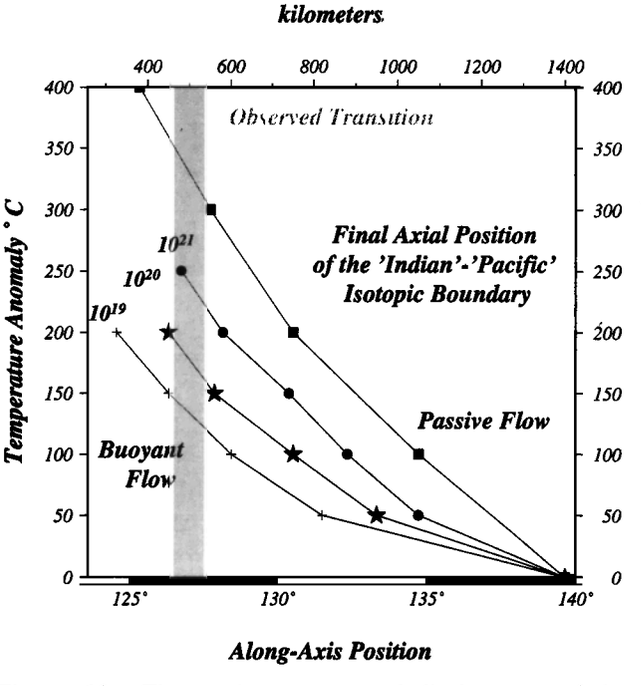

Figure 12. The maximum westward displacement of the Pacific-Indian isotopic boundary as predicted from the advection relationship described by (4) for all variable viscosity simulations. The notation is as shown in Figure 11. Shaded area shows the observed location of the Indian to Pacific isotopic transition observed on axis [*Pyle et al.,* 1992]. Higher along-axis flow velocities produced by larger mantle temperature anomalies (Figure 11) result in the increased westward advection of the isotopic boundary. In models that include buoyancy, the temperature anomaly required to reproduce the observed location is significantly reduced since buoyancy enhances upwelling in warmer regions outside the AAD, thereby resulting in increased lateral advection of the isotope boundary.

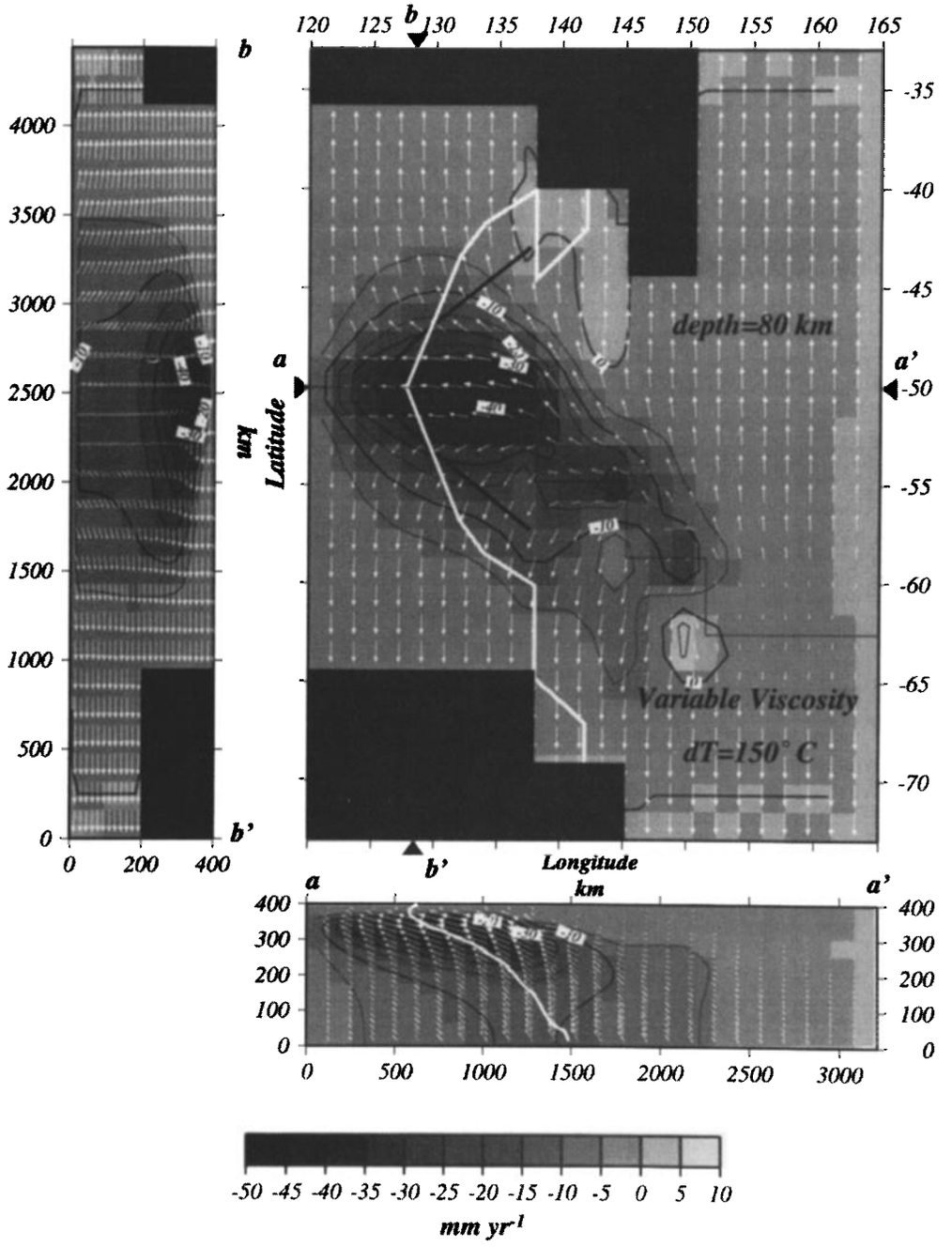

Figure 13. Planform of present-day buoyant upper mantle flow due to the separation of the Australian and Antarctic continents in a mantle with a temperature- and pressure-dependent viscosity and a horizontal basal temperature gradient. In this simulation, the influx temperature decreases linearly from 1400°C at 145°E to 1250°C at 120°E, and the reference upper mantle viscosity μ_o is 10^{20} Pa s. The planform of this simulation is similar to the results of the passive flow simulations with a 300°C temperature anomaly (Figure 8). The temperature anomaly required to reproduce the propagating rift traces (black line) and distribution of the isotope boundary at depth (white line) is significantly less than the 300°C required by solely passive flow and is more consistent with other geophysical and geochemical estimates of the temperature anomaly.

the observed distribution of isotopic provinces, and along-axis variations in residual depth and crustal thickness. We find that in the absence of temperature anomalies within the upper mantle beneath the AAD, the divergence of the Australian and Antarctic continents induces along-axis flow of material in both constant and variable rheologic conditions. However, this flow is insufficient to match the along-axis flow velocity of about 30-45 mm yr^{-1} required by geophysical and geochemical constraints. Our models demonstrate that variations in upper mantle temperatures in a variable-viscosity model can induce along-axis flow velocities of sufficient magnitude to result in the advection of Pacific type upper mantle to its observed position within the AAD and match flow velocities suggested by the off-axis trace of propagating rifts. When buoyancy forces are included, a mantle temperature anomaly beneath the AAD of between 100°

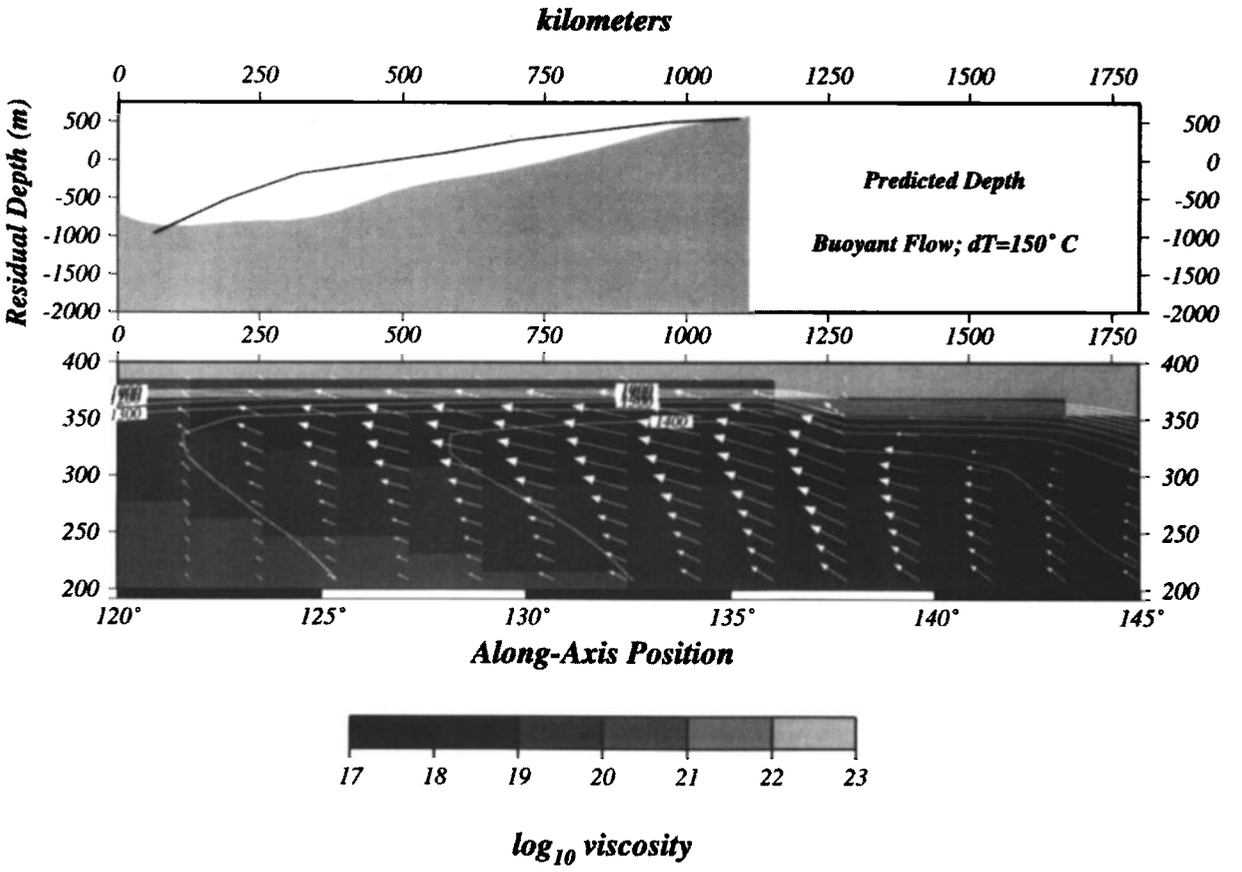

Figure 14. Vertical along-axis section including the SEIR between 120°E and 136°E for a simulation including buoyancy forces and a temperature anomaly of 150°C in the upper mantle beneath the AAD (Figure 12). The reference upper mantle viscosity μ_0 is 10^{20} Pa s. The notation is the same as Figure 10. The subaxial planform of flow beneath the ridge axis is similar to simulations that do not include buoyancy forces; along-axis flow advects warmer asthenosphere into the shallow low-viscosity zone overlying cooler, deeper regions and produces a temperature inversion in the subaxial asthenosphere. The viscosity variation required to drive horizontal flow is less due to the reduced temperature anomaly and the addition of buoyancy forces that retard upwelling beneath the AAD. The predicted along-axis change in axial depths matches the observed residual depth anomaly reasonably well.

and 200°C is required to match geophysical and geochemical constraints from this region. Our models also demonstrate that hotspot driving forces [*Marks et al.*, 1990, 1991], a "push" from a shrinking Pacific Ocean basin [*Alvarez*, 1982, 1990], or actual mantle downwelling in the shallow (< 400 km) upper mantle beneath the AAD [*Marks et al.*, 1991] are not required to match these first-order constraints.

The AAD has been proposed as a location of large-scale mantle downwelling beneath the global ridge system based on geoid to topography ratios from this region and patterns of residual depth anomalies [*Marks et al.*, 1990, 1991]. Anomalously cool upper mantle beneath the AAD does result in a negative buoyancy force which tends to retard upwelling in this region. However, our simulations show that actual downwelling is not required within the upper 400 km to reproduce the geophysical and geochemical constraints. Our results suggest that the mantle beneath the AAD is not downwelling but, rather, upwelling more slowly than the surrounding mantle beneath the SEIR (Figures 10 and 14). Slower upwelling of cool mantle would result in lower extents of decompressional melting, consistent with geochemical signatures of basaltic samples taken from this region [*Pyle*, 1994] and an overall reduced magma supply rate required by thinner crust beneath the AAD [*West et al.*, 1994; *Tolstoy et al.*, 1995]. A more slowly upwelling mantle within the AAD results in what might be termed "relative" downwelling. *Kuo et al.* [1995] also suggest that suppressed upwelling beneath the AAD can match the large-scale topographic and geoid data. Indeed, the production of zero-age basalts within the AAD seems infeasible if the mantle is actually downwelling in this region.

The models we have constructed are dependent on both constraints from the geophysical and geochemical data. Although our flow models are able to match the observed distribution of the Indian-Pacific isotopic boundary and the subaxial flow velocities inferred from propagating ridges with reasonable upper mantle temperature variations, alternative explanations exist for both of these constraining phenomena. In the following sections, we discuss some of the fundamental constraints on our simulations and, finally, speculate on the possible ramifications of along-axis flow on geochemical processes beneath the SEIR.

Migration of the Isotopic Boundary

The position and behavior of the Indian-Pacific isotopic boundary at a depth of 400 km is the least well constrained

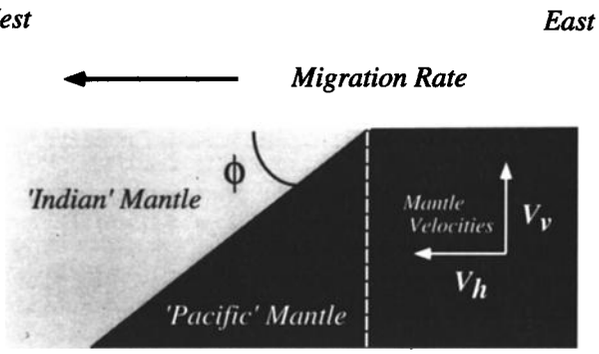

Figure 15. Schematic diagram of mantle flow in the plane of the ridge axis and apparent migration rate of an isotopic boundary that is inclined throughout the mantle. The geometrical relationships are described in (7). Vertical upwelling of a boundary dipping to the west can produce apparent westward migration of the Pacific isotopic upper mantle province, thus reducing the required mantle temperature anomaly shown in Figure 12.

boundary conditions and we have chosen to fix the boundary at the base of our model. Our assumption is necessarily speculative because our knowledge of the subsurface distribution of isotopic provinces is non-existent. The westward migration of the isotope boundary described by *Pyle et al.* [1992, 1995] and *Lanyon et al.* [1995] could be produced by purely vertical upwelling of a boundary between Indian and Pacific provinces that is inclined throughout the upper mantle (Figure 15). Assuming only vertical passive flow due to plate separation, an "apparent" migration velocity of 25 mm yr^{-1} within the AAD (37 mm yr^{-1} half rate) requires a boundary dipping about 40° to the west. This end-member configuration is unlikely since it would require a boundary that sloped to a depth of approximately 2000 km at 40 Ma, and it is unclear whether it would be possible to sustain this geometry to the present day. However, in a mantle with both vertical and along-axis components of flow, an isotopic boundary that dips at a steeper angle ϕ toward the west (Figure 15) can reproduce the apparent migration rate recorded, if the upper mantle along-axis flow velocities are insufficient to advect an isotopic "front" from within the Tasman transform complex to a location within the AAD. The dip that is required to reproduce the apparent migration rate for arbitrary upper mantle flow velocities is:

$$\phi = \tan^{-1}\left(\frac{(V_v)}{(M_r)-(V_h)}\right) \quad (7)$$

where V_v is the vertical component, M_r is the migration rate, and V_h is the along axis component. A sloped boundary between the Indian and Pacific isotopic reservoirs would reduce the temperature anomaly required to reproduce the advection of the isotopic boundary into the AAD (Figure 12). For instance, for along-axis flow velocities of 30 mm yr^{-1} superimposed on a passive flow solution (V_v=23 mm yr^{-1}), an isotopic migration velocity of 40 mm yr^{-1} requires an angle of 66°. In addition to a sloped boundary, a vertical boundary between isotopic provinces oriented northwest to southeast across the ocean basin could also result in the westward along-axis migration of the boundary since the SEIR is moving northward in a hotspot reference frame. These geometric considerations show that significant along-axis mantle flow beneath the SEIR, as described by *Pyle et al.* [1995], is not the only means to reproduce the migration of the isotopic boundary: simple perturbations to subsurface boundary geometry can reduce the magnitude of along-axis flow required to explain the isotopic boundary migration [*Pyle et al.*, 1995].

Pyle et al. [1995] assume that the isotopic boundary migrated at a constant rate from Tasmania to its current location within the AAD and estimate a migration velocity of 40 mm yr^{-1}. Our results demonstrate that it is possible for a particle entering our numerical domain at a depth of 400 km and near 142°E to be advected into the AAD if temperature anomalies beneath the AAD are about 150°C. However, our model does not predict a constant migration velocity through time (Figures 8 and 13). Initially high along-axis flow velocities advect the isotopic boundary rapidly towards the AAD. After about 30 Ma, the along-axis flow pattern stabilizes and the migration velocity decreases since we have fixed the location of the isotopic boundary at the bottom of the domain. Our flow model is consistent with currently available data. However, further off-axis constraints on the isotopic boundary position between 128°E and the Tasman fracture zone will be required to determine the relative contributions of along-axis flow and geometrical effects.

Propagating Rifts and Along-Axis Asthenospheric Flow

To constrain the magnitude of along-axis flow, we assumed that the migration velocities of propagating rifts reflect of along axis asthenospheric flow through the melt column, thereby ignoring lithospheric/asthenospheric interaction. Using this assumption, the calculated trajectories of a perpetuating melting anomaly traveling along-axis at a depth of 50 km over the last 25 Myr are plotted in Figures 6, 7, 8, and 13. Whether propagating rifts travel with along-axis mantle flow, as we have assumed, or are simply driven by segment-scale topographic gradients [*Phipps Morgan and Parmentier,* 1985] is, at present, poorly understood. Both processes may be important. However, if propagating rifts simply traverse topographic gradients [*Phipps Morgan and Parmentier,* 1985] and are not directly related to along-axis flow, the presence of multiple propagating ridges convergent upon the AAD from both the east and west along the SEIR may still require large-scale, along-axis flow toward the AAD. Mid-ocean ridge segments are commonly characterized by midsegment topographic highs which trend into deeps at the segment ends. If lithospheric segmentation is related to mantle segmentation at some level, then along-axis flow of asthenosphere will also advect the mid-ocean ridge segment and the associated topographic gradient along axis [*Schouten et al.*, 1987]. In this case, the propagating ridges will respond to along-axis flow, but the asthenospheric migration rate obtained by measuring pseudofault traces may not be equal to the velocity of along-axis flow.

Cool Upper Mantle Temperatures and V-Shaped Residual Depth Anomaly

Marks et al. [1990, 1991] infer that the residual depth anomaly has migrated to the west over the past 40 Myr at rate of between 15 and 25 mm yr^{-1} and suggest that the magnitude of the residual depth anomaly has increased in strength over the last 30 Myr. In constraining the models of along-axis flow beneath the SEIR, we have assumed that the westward asthenospheric flow occurs in response to more viscous

conditions at depth beneath the AAD. Further, we have fixed the mantle temperature gradient and assumed a fixed "stagnation" point for along-axis flow at 120°E, the center of the cooler than normal upper mantle temperatures [*Kuo et al.*, 1996]. It would be pointless for us to refine our model further to match the migration rate and intensity of the residual depth anomaly since these characteristics are essentially determined *a priori* by the bottom temperature boundary condition. Our models do show appreciable along-axis flow at 400 km depth, even quite close to the AAD (Figures 10 and 14). It can be argued that this flow would tend to steepen the along-axis temperature gradients and compress the margins of the AAD. Indeed, the residual depth anomaly does appear to have a slight "hourglass" shape superimposed upon the V shape resulting from westward migration (Figure 4). However, such arguments are very speculative because the initial geometry of the mantle thermal anomaly causing the AAD is completely unconstrained.

Along-Axis Asthenospheric Flow and Melting Beneath the SEIR

We demonstrate that gradients in upper mantle temperatures strongly influence the structure of flow in a temperature- and pressure-dependent viscosity regime. Although focused on a much more localized scale than that which we address, *Vogt and Johnson* [1975] also examine the structure and effect of "longitudinal" asthenospheric flow beneath mid-ocean ridges. They propose that transform faults offset the "pipe-shaped" region of partial melting and magma generation beneath mid-ocean ridges and therefore act as impediments to longitudinal flow below mid-ocean ridges. Our models of the migration of Pacific upper mantle into the Indian Ocean through the Tasman Transform Complex imply that under the influence of regional mantle temperature variations significant transform offsets do not hinder large-scale upper mantle flow, although our numerical geometry may lack the resolution to address many of the arguments that *Vogt and Johnson* [1975] present.

On more regional scales, variations in upper mantle temperature structure have been demonstrated to significantly influence the volume [*Su et al.*, 1994; *West et al.*, 1994] and composition [*Klein and Langmuir*, 1987] of adiabatic decompressional melts. In regions that contain significant along-axis flow, our models predict that warmer upper mantle can be advected into the low-viscosity region beneath the ridge axis (Figures 10 and 14). The low-viscosity region also corresponds to the melting region beneath mid-ocean ridges, and thus warmer upper mantle will be advected into the melting region. This process results in the presence of relatively warmer upper mantle within the melt column overlying a relatively cooler deeper mantle (Figure 10 (bottom) and Figure 14 (bottom)) and thus subdues the effects of regional along-axis temperature variations. The net effect is to produce a temperature inversion in the subaxial mantle so that temperatures in the shallow mantle are warmer than would be expected from simple two-dimensional upwelling.

In addition to placing warmer asthenosphere over cooler mantle, our models suggest that significant along-axis motion of residuum mantle occurs within the melting region beneath the ridge axis owing to the regional mantle temperature variations. Assuming melt segregates from the matrix at moderate depths within the melting column, this scenario also departs from the a two-dimensional melt column where both residuum and partial melt remain in the same vertical plane. In our model, residuum within the melting column follows a complex path through the melting region and results in a "tilted" residual column.

Assuming that the depth of compensation of mid-ocean ridges extends to approximately 100-200 km [*Forsyth*, 1992], average axial depths will be dependent on the integral of the warmer overlying and cooler underlying mantles (Figures 10 and 14). On the other hand, the melting process will reflect only the presence of warmer mantle within the melting region. The combined result would lead to higher extents of melting, lower $Na_{8.0}$, higher $Fe_{8.0}$ values, and shallower axial depths than would be observed in the absence of along-axis flow. Further, the advection of already-melted mantle into the cooler regions would result in a relatively more depleted overlying melt column. The net result would be a muting of the "global correlation" between $Na_{8.0}$, $Fe_{8.0}$, and axial depth reported by *Klein and Langmuir* [1987] in regions where temperature-driven, along-axis asthenospheric flow exists (Figure 16). Such a signal may be observed in the SEIR between 89° and 112°E, which shows significant variation in axial depth at a constant spreading rate, yet smaller variations in $Na_{8.0}$ and $Fe_{8.0}$ than would be expected from a simple global correlation viewpoint [*Christie et al.*, 1995].

Conclusions

1. Separation of the Australian and Antarctic continents can result in a significant along-axis component of asthenospheric flow, consistent with the westward migration of propagating ridges and Indian-Pacific isotopic boundary if anomalously cool upper mantle temperatures beneath the AAD are present. Hotspot driving forces, a push from a shrinking Pacific Ocean basin, or actual mantle downwelling in the

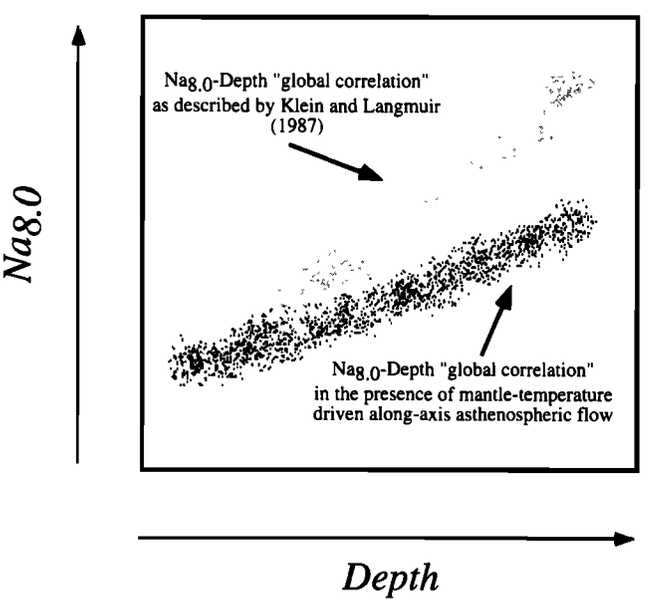

Figure 16. Hypothetical trends showing the correlation between regional average Na_2O contents of lavas (expressed as $Na_{8.0}$, the Na_2O content normalized to 8% MgO to eliminate shallow crystallization effects) and regional average depth at the spreading axis in a normal ridge environment (gray) and in the presence of mantle-temperature-driven along-axis flow (black).

shallow (<400 km) upper mantle beneath the AAD are not required to match existing first-order constraints from both geochemical and geophysical data. If this flow is driven solely by continental separation and passive inflow of Pacific mantle due to cooler, more viscous mantle conditions within the AAD, the required temperature anomaly is about 300°C. Such a temperature anomaly is incompatible with the temperature anomaly estimated by previous studies. The introduction of buoyancy forces decreases the required temperature variation, and we predict that temperature anomalies beneath the AAD are about 100-200°C (depending on the viscosity of the mantle).

2. The symmetry of our model around 120°E implies that cooler upper mantle temperatures in this region will result in significant along-axis flow toward the AAD beneath the SEIR from the east and west and a reduction in mantle upwelling beneath the AAD, consistent with the geochemical and geophysical characteristics of the AAD.

3. Our results demonstrate that in regions that contain significant along-axis flow, warmer upper mantle will be advected into the low-viscosity region beneath the ridge axis. This process results in the presence of relatively warmer, low-viscosity material within the shallow mantle overlying cooler, more viscous, deeper regions. For example, a horizontal temperature anomaly of 150°C at a depth of 400 km (with $\mu_0=10^{20}$ Pa s) produces a horizontal temperature anomaly within the melting region of only about 75°C. This process may be responsible for the anomalously low sensitivity of parameters such as $Na_{8.0}$ to axial depth between 98° and 116°E reported by *Christie et al.* [1995].

4. The presence of the sub-axial temperature inversion may reconcile differences between geochemical and geophysical estimates of the mantle temperature anomaly associated with the AAD. Geochemical estimates range from 60° to about 150°C. Geophysical estimates (predominately seismic), on the other hand, range from 100° to values greater than 250°C. Since geochemical estimates will by definition reflect the mantle temperature within the melting region, while geophysical estimates reflect both the temperature within the melting region and underlying mantle, the sub-axial temperature inversion may explain why geochemical estimates are consistently less than geophysical and seismic estimates of the AAD's temperature anomaly.

5. Our results support the conclusions of other workers that the anomalous geochemical and geophysical character of the AAD, the migration of the isotopic boundary, and the paths of propagating ridges along the SEIR result from the presence of anomalously cooler upper mantle in this region (e.g., the residual depth anomaly) [*Weissel and Hayes,* 1974; *Forsyth et al.,* 1987; *Marks et al.,* 1991; *Kuo* 1993; *Kuo et al.,* 1995; *Pyle,* 1994; *West et al,* 1994, also manuscript in preparation, 1997 *Sempéré,* 1997].

Acknowledgments. All calculations were performed on a DEC Alpha 3000/600 owned and maintained by the Volcanic Systems Center (VSC) at the University of Washington. We would like to thank J. Delaney and VSC for their continuing support of our efforts in the Southern Ocean. Extensive discussions with D. Christie, D. Pyle, D. Graham, and B. Nelson have contributed significantly to this work. We thank J. Phipps Morgan and B.-Y. Kuo for making data available to us for use in Figure 1. We also thank G. Ito, Y. Shen, R. Kinzler, and Y. J. Chen for their thoughtful reviews of the original manuscript. This study was supported by National Science Foundation grants OCE-9420649 and OCE-9403583 and an Office of Naval Research Graduate Fellowship award to B. P. West. L. Géli would also like to thank IFREMER for its support during his 1995 sabbatical year at the University of Washington.

References

Alvarez, W., Geological evidence for the geographical pattern of mantle return flow and the driving mechanism of plate tectonics, *J. Geophys. Res., 87*, 6697-6710, 1982.

Alvarez, W., Geologic evidence for the plate driving mechanism: The continental undertow hypothesis and the Australian-Antarctic Discordance, *Tectonics, 9*, 1213-1220, 1990.

Batchelor, G. K., *An Introduction of Fluid Dynamics*, Cambridge Univ. Press, New York, 1967.

Baumgardner, J., 3-D numerical investigation of mantle dynamics with circum-Pangea subduction as an initial condition (abstract), *Eos Trans. AGU, 69*, 1414, 1988.

Blankenbach, B. F., et al., A benchmark comparison for mantle convection codes, *Geophys. J. Int., 98*, 23-38, 1989.

Cande, S.C., and J.C. Mutter, A revised identification of the oldest sea-floor spreading anomalies between Australia and Antarctica, *Earth Planet. Sci. Lett., 58*, 151-160, 1982.

Cathles, L. M., *The Viscosity of the Earth's Mantle*, Princeton Univ. Press, Princeton, N. J., 1975.

Chen, Y. J., Constraints on the melt production rate beneath the mid-ocean ridges based on passive flow models, *Pure Applied Geophys., 156*, 590-620, 1996a.

Chen, Y. J., Dynamics of the Mid-Ocean Ridge plate boundary: Recent observations and theory, *Pure Applied Geophys., 146*, 621-648, 1996b.

Christie, D. M., B. Sylvander, and F. Sprtel, Major element variability of basalts from the Southeast Indian Ridge between 88°E and 118°E (abstract) *Eos Trans. AGU, 76*, (46), Fall Meet. Suppl., F529, 1995.

Cooper, R. R. , and D. L. Kohlstedt, Rheology and structure of olivine-basalt partial melts, *J. Geophys. Res., 91*, 9315-9323, 1986.

Forsyth, D. W., Geophysical constraints on mantle flow and melt generation beneath mid-ocean ridges, *Mantle Flow and Melt Generation at Mid-Ocean Ridges, Geophys. Monogr. Ser.*, vol. 71, edited by J. Phipps Morgan, D. Blackman, and J. Sinton, pp. 1-65, AGU, Washington, D. C., 1992.

Forsyth, D. W., R. L. Ehrenbard, and S. Chapin, Anomalous upper mantle beneath the Australian-Antarctic Discordance, *Earth Planet. Sci. Lett., 84*, 471-478, 1987.

Goetze, C., The mechanisms of creep in olivine, *Philos. Trans. R. Soc. London, Ser. A., 288*, 99-119, 1978.

Guillou, L., and C. Jaupart, On the effect of continents on mantle convection, *J. Geophys. Res., 100*, 24,217-24,238, 1995.

Hayes, D. E., Age-depth relationships and depth anomalies in the Southeast Indian Ocean and South Atlantic Ocean, *J. Geophys. Res., 93*, 2937-2954, 1988.

King, S., A. Raefsky, and B.H. Hager, ConMan: Vectorizing a Finite Element code for incompressible two dimensional convection in the Earth's mantle, *Phys. Earth Planet. Inter., 59*, 195-207, 1989.

Klein, E.M., and C.H. Langmuir, Global correlations of ocean ridge basalt chemistry with axial depth and crustal thickness, *J. Geophys. Res., 92*, 8089-8115, 1987.

Klein, E.M., C.H. Langmuir, A. Zindler, H. Staudigel, and B. Hamelin, Isotope evidence of a mantle convection boundary at the Australian-Antarctic discordance, *Nature, 333*, 623-629, 1988.

Kuo, B.-Y., Thermal anomalies beneath the Australian-Antarctic Discordance, *Earth Planet. Sci. Lett., 119*, 349-364, 1993.

Kuo, B. Y., S. H. Hung, and L. Y. Chiao, A 3-D dynamic model for the anomalous topography and geoid over the Southeast Indian Ridge, *Geophys. J. Int., 121*, 1-20, 1995.

Kuo, B.-Y., C.-H. Chen, and Y.-S. Zhang, A fast velocity anomaly to the west of the Australian-Antarctic Discordance, *Geophys. Res. Lett., 23*, 2239-2243, 1996.

Lanyon, R., A.J. Crawford, and S.M. Eggins, Westward migration of Pacific Ocean upper mantle into the Southern Ocean region between Australia and Antarctica, *Geology, 23*, 511-514, 1995.

Lawver, L.A., L.M. Gahagan, and M.F. Coffin, The development of paleoseaways around Antarctica, in *The Antarctic Paleoenvironment: A Perspective on Global Change, Antarc. Res. Ser.*, vol. *56*, edited by J.P. Kennett and D. A. Warnke, pp. 7-30, AGU, Washington, D.C., 1992.

Marks, K. M., P. R. Vogt, and S. A. Hall, Residual depth anomalies and the origin of the Australian-Antarctic Discordance zone, *J. Geophys. Res., 95*, 17325-17338, 1990.

Marks, K. M., D. T. Sandwell, P. R. Vogt, and S. A. Hall, Mantle downwelling beneath the Australian-Antarctic Discordance zone: Evidence from geoid height versus topography, *Earth Planet. Sci. Lett., 103*, 325-338, 1991.

McKenzie, D. P., The generation and compaction of partially molten rock, *J. Petrol., 25*, 713-765, 1984.

Mutter, J.C., K.A. Hegarty, S.C. Cande, and J.K. Weissel, Breakup between Australia and Antarctica: A brief review in the light of new data, *Tectonophysics, 114*, 255-279, 1985.

Ogawa, M., G. Schubert, and A. Zebib, Numerical experiments of three-dimensional thermal convection in a fluid with strongly temperature dependent viscosity, *J. Fluid Mech., 233*, 299-328, 1991.

Palmer, J., J.-C. Sempéré, J. Phipps Morgan, and D. Christie, Morphology and tectonics of the Australian-Antarctic Discordance, *Mar. Geophys. Res., 15*, 121-152, 1993.

Parmentier, E. M., and J. E. Oliver, A study of shallow global mantle flow due to the accretion and subduction of lithosphere plates, *Geophys. J. Roy. Astr. Soc., 57*, 1-21, 1979.

Patankar, S. V., *Numerical Heat Transfer and Fluid Flow*, 197 pp., Hemisphere, New York, 1980.

Phipps Morgan, J., and D. W. Forsyth, Three-dimensional flow and temperature perturbations due to a transform offset: Effects on oceanic crustal and upper mantle structure, *J. Geophys. Res., 93*, 2955-2966, 1988.

Phipps Morgan, J., and Y. J. Chen, The dependence of ridge-axis morphology and geochemistry on spreading rate and crustal thickness, *Nature, 364*, 706-708, 1993.

Phipps Morgan, J., and E. M. Parmentier, Causes and rate-limiting mechanisms of ridge propagation: A fracture mechanics model, *J. Geophys. Res., 90*, 8603-8612, 1985.

Phipps Morgan, J., and D. T. Sandwell, Systematics of ridge propagation south of 30°S, *Earth Planet. Sci. Lett., 121*, 245-258, 1994.

Pyle, D.G., Geochemistry of mid-ocean ridge basalt within and surrounding the Australian-Antarctic Discordance, Ph.D. dissertation, 178 pp., Oreg. State Univ., Corvallis, 1994.

Pyle, D.G., D.M. Christie, and J.J. Mahoney, Resolving an isotopic boundary within the Australian-Antarctic Discordance, *Earth Planet. Sci. Lett., 112*, 161-178, 1992.

Pyle, D.G., D.M. Christie, and J. J. Mahoney, Geochemistry and geochronology of ancient southeast Indian and southwest Pacific seafloor, *J. Geophys. Res., 100*, 22,261-22,282, 1995.

Rabinowicz, M., S. Rouzo, J.-C. Sempéré, and C. Rosemberg, Three-dimensional mantle flow beneath mid-ocean ridges, *J. Geophys. Res., 98*, 7851-7869, 1993.

Reid I., and H.R. Jackson, Oceanic spreading rate and crustal thickness, *Mar. Geophys. Res., 5*, 165-172, 1981.

Roult, G., D. Rouland, and J.-P. Montagner, Antarctica, II; Upper mantle structure from velocities and anisotropy, *Phys. Earth. Planet. Inter., 84*, 33-57, 1994.

Schouten, H., H.J.B. Dick, and K. D. Kiltgord, Migration of mid-ocean ridges, *Nature, 326*, 835-839, 1987.

Sempéré, J.-C., B. P. West, and L. Géli, The Southeast Indian Ridge between 127° and 133°E: Contrasts in segmentation characteristics and implications for crustal accretion, *Tectonic, Magmatic, Hydrothermal and Biological Segmentation of Mid-Ocean Ridges, Geological Society Special Publication No. 118*, edited. by C McLeod and C. Walker, Geol. Soc., London, 1996

Sempéré, J.-C., J. R. Cochran, and the SEIR scientific team, The Southeast Indian Ridge between 88°E and 118°E: variations in crustal accretion at constant spreading rate, *J. Geophys. Res.*, in press, 1997.

Shen, Y., and D. W. Forsyth, Geochemical constraints on initial and final depths of melting beneath mid-ocean ridges, *J. Geophys. Res., 100*, 2211-2237, 1995.

Smith, W.H.F, and D. T. Sandwell, Marine gravity field from declassified GEOSAT and ERS-1 altimetry (abstract), *Eos Trans. AGU, 76*, (46), Fall Meet. Supp., F156, 1995.

Spalding, D. B., *Combustion and Mass Transfer*, Pergamon, Tarrytown, N. Y., 1979.

Spalding, D. B., Mathematical modeling of fluid-mechanics, heat-transfer and chemical-reaction processes: A lecture course, *Imperial College CFDU Rep. HTS/80/1*, Imperial Coll., London, 1980.

Su, W., C. Mutter, J. C. Mutter, and W. R Buck, Some theoretical predictions on the relationships among spreading rate, mantle temperature and crustal thickness, *J. Geophys. Res., 99*, 3215-3227, 1994.

Tolstoy, M., A. J. Harding, J. A. Orcutt, and J. Phipps Morgan, A seismic refraction investigation of the Australian-Antarctic Discordance and neighboring Southeast Indian Ridge: Preliminary results (abstract), *Eos Trans. AGU, 76*, (46), Fall Meet. Supp., F570, 1995.

Turcotte, D.L. and G. Schubert, *Geodynamics: Applications of Continuum Physics to Geological Problems*, John Wiley, New York, 1982.

Veevers, J.J., Australian-Antarctic depression from the mid-ocean ridge to adjacent continents, *Nature, 295*, 315-317, 1982.

Vogt, P.R., and G.L. Johnson, Transform faults and longitudinal flow below the mid oceanic ridge, *J. Geophys. Res., 80*, 1399-1428, 1975.

Vogt, P.R., N.K. Cherkis, and G.A. Morgan, Project Investigator, Evolution of the Australian-Antarctic Discordance from a detailed aeromagnetic study, in *Antarctic Earth Science: Proceedings of the 4th International Symposium on Antarctic Earth Sciences*, edited by R.L. Oliver, P.R. James, and J. Jago, pp. 608-613, Aust. Acad. of Sci., Canberra, 1984.

Weissel, J.K. and D.E. Hayes, The Australian-Antarctic Discordance: New results and implications, *J. Geophys. Res., 79*, 2579-2587, 1974.

West, B.P., and J-C. Sempéré, Gravity Anomalies, Flexure of Axial Lithosphere, and Along-Axis Mantle Flow Between 98° and 112° E on the Southeast Indian Ridge, *Earth Planet. Sci. Lett.*, in press, 1997.

West, B.P., J.-C. Sempéré, D.G. Pyle, J. Phipps Morgan, and D. M. Christie, Evidence for variable upper mantle temperature and crustal thickness in and near the Australian-Antarctic Discordance, *Earth Planet. Sci. Lett., 128*, 135-153, 1994.

L. Géli, Département de Géosciences Marines, Institut Français de Recherche pour l'Exploitation de la Mer, B. P. 70, 29280 Plouzané, France.

J.-C. Sempéré, Exxon Production Research Company, P. O. Box 2819, Houston, TX 77252-2189.

B. P. West and W. S. D. Wilcock, School of Oceanography, University of Washington, P. O. Box 357940, Seattle, WA 98195-7940. (e-mail: bpw@ocean.washington.edu).

(Received June 19, 1996; revised December 5, 1996;
accepted December 11, 1996.)